Stony Brook University

OFFICIAL COPY

The official electronic file of this thesis or dissertation is maintained by the University Libraries on behalf of The Graduate School at Stony Brook University.

© All Rights Reserved by Author.

Radiation Damage Study Of A DPP Polymer Using Transmission Electron Microscope

A Thesis Presented

by

Sai Bharadwaj Vishnubhotla

to

The Graduate School

in Partial Fulfillment of the

Requirements

for the Degree of

Master of Science

in

Materials Science and Engineering

Stony Brook University

May 2015

Stony Brook University

The Graduate School

Sai Bharadwaj Vishnubhotla

We, the thesis committee for the above candidate for the

Master of Science degree, hereby recommend

acceptance of this thesis.

Dr. Huolin Xin– Thesis Advisor
Staff Scientist, Electron Microscopy Group
Center for Functional Nanomaterial (CFN)
Brookhaven National Laboratory (BNL)

Dr. Dilip Gersappe – Committee Chairperson
Professor, Graduate Program Director
Materials Science and Engineering Department

Dr. Balaji Raghothamachar – Committee member
Research Assistant Professor
Materials Science and Engineering Department

This thesis is accepted by the Graduate School

Charles Taber
Dean of the Graduate School

Abstract of the Thesis

Radiation Damage Study Of A DPP Polymer Using Transmission Electron Microscope

by

Sai Bharadwaj Vishnubhotla

Master of Science

in

Materials Science and Engineering

Stony Brook University

2015

In general polymeric materials are sensitive to the electron beam in the transmission electron microscopes (TEM). Radiolysis or ionization is the primary mechanism by which these materials are damaged under electron irradiation. Moreover, the image resolution of these materials in a TEM is determined by radiation damage. In the following work we determine the radiation sensitivity and damage mechanism for a single crystal organic material 3,6-bis (5-(4-n-butylphenyl) thiophene-2-yl)-2,5-bis (2-ethylhexyl) pyrrolo[3,4-c]pyrrole-1,4-dione (DPP-PR) majorly used for organic photovoltaic (OPV) applications as a donor material. We provide a complete experimental and analysis procedure for radiation damage study by utilizing electron diffraction patterns. First at 120KeV, we learn that the critical dose value doesn't change significantly with the dose rate. The critical dose is independent of the dose rate. Second, we experimentally determine critical dose (D_e) values 3 ($\frac{e^-}{A^{o2}}$) and 6 ($\frac{e^-}{A^{o2}}$) at electron energies of 120KeV and 200KeV respectively. We find the increase in the value of the critical dose, which indicates an increase in the resistance of the material to radiation damage at higher electron

energies. The ionization mechanism causes the breakage of the bonds of the DPP polymer leading to the loss of crystalline structure. We also conducted the experiment at low temperature of -175℃ at 120KeV. And the determined critical dose value is $8(\frac{e^-}{A^{o2}})$. Hence we confirm that reducing the temperature is effective to reduce radiation damage for the polymers.

Keywords: TEM, Polymers, Elastic and Inelastic scattering, Electron Diffraction, Radiation Damage.

Table of Contents

List of Figures

List of Tables

List of Abbreviations

TEM	Transmission Electron Microscope
DPC	Droplet-Pinned Crystallization

Acknowledgments

I am extremely grateful to Dr.Huolin Xin for his guidance, support and training at Center for functional nanomaterial (CFN), Brookhaven National Laboratory (BNL).

I am thankful to Dr.Dilip Gersappe and Dr.Balaji Raghothamachar for their suggestions.

I am thankful to all the department faculty and staff for their continuous supervision.

I also thank my parents, sister, colleagues and friends for their caring and support.

Chapter 1

Radiation Damage

1.1 Interactions of electrons with the matter

In nature, we can see things because of the scattering of light by the matter. Similarly in the transmission electron microscope (TEM) we observe and get information from the scattering of electrons from the specimen. In general there are two types of scattering, which are elastic scattering and inelastic scattering.

Electrons get elastically scattered due to the coulombic attraction of the nucleus. We assume here that there isn't any measurable loss of the energy. The elastic scattering also constitutes for the intensities in a diffraction pattern (DP), which are obtained in a TEM.

Inelastic scattering of electrons takes place due to coulombic interactions of electrons with the atomic electrons around the nucleus. Also, inelastic scattering causes damage in beam sensitive specimens.

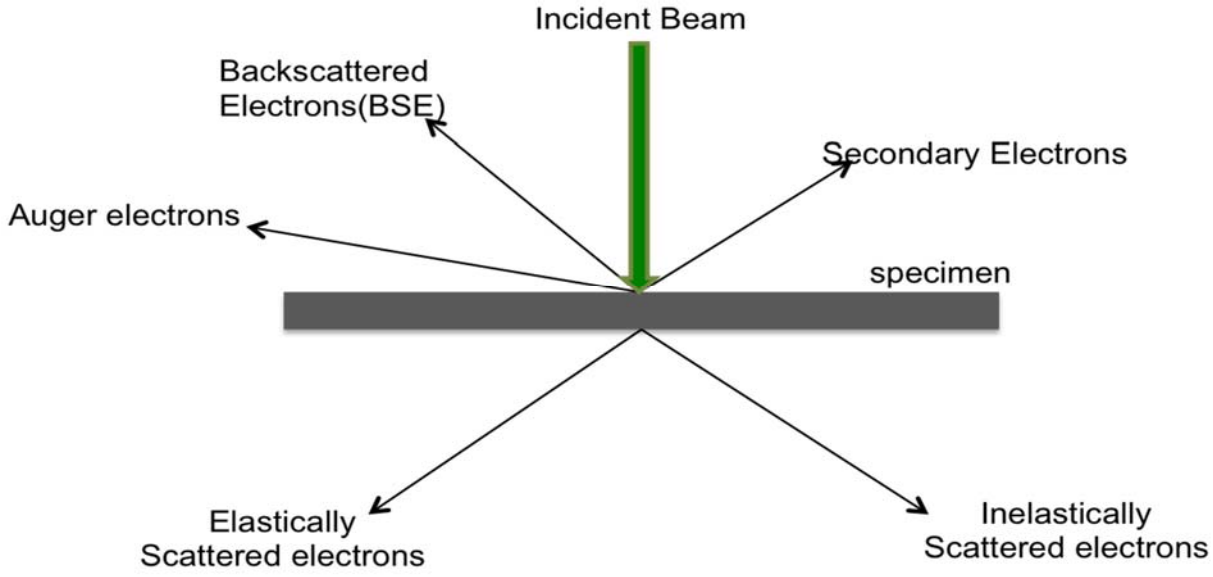

Figure 1. Interactions of electrons with matter in the TEM.

From inelastic scattering, we can gain electron-energy loss spectroscopy (EELS) information, which is useful for radiation damage studies. These two types of scattering are crucial for the characterization of materials in TEM[1].

1.2.Scattering cross section and mean free path

We a need single scattering event to occur in the TEM for the good interpretation of images and diffraction Patterns. The higher the scattering, the more difficult it is to interpret the information. We quantify the scattering in terms of scattering cross-section (σ). The greater the cross-section, the greater is the probability for the scattering event to occur. Scattering from the specimen can be written as

$$\sigma_{total} t = \frac{N_0 \sigma_{atom} (\rho t)}{A}$$

where N_0 is Avogadro number($atoms\ mol^{-1}$), A is atomic weight ($kg\ mol^{-1}$) and ρ is density ($Kg\ m^{-3}$).

We represent the interactions in terms of mean free path because it gives us measure in terms of the length. The mean free path is defined as the average distance an electron travels between the scattering events. The expression for mean free path is

$$\lambda = \frac{1}{\sigma_{total}} = \frac{A}{N_0 \sigma_{atom} \rho}$$

The value comes in the range of nanometers (nm) and is useful in determining the sample thickness of the specimen[2].

The electron scattering decreases as the incident energy of electrons increases say from 100KV to 300 KV. We shall see that for beam sensitive specimens like polymers it has important significance. In this thesis, we will measure radiation sensitivity of a particular polymer (DPP-PR) at electron energies of 120KeV and 200KeV.

1.3 Radiation Damage

1.3.1 Definition

In Electron Microscopy, radiation damage is defined as causing a temporary or permanent change to surface or bulk of the specimen. The damage can be a change in structure, chemistry etc., and the information we get from TEM is no longer from the desired material. Radiation damage dosage is defined in terms of Grays, which is absorption 1 J of ionizing radiation per Kg of materials. This term is used for dosage in the experiments utilizing x-rays. Whereas in TEM, electron dose is represented in terms of charge density (C/m^2) exposed on to the specimen. We shall convert this into ($e^-/A^{\circ 2}$) and use this unit for electron dose thought the experiments.

The radiation damage in materials is characterized based on elastic and inelastic scattering. The basic types of damage are radiolysis, knock-on damage, and heating. Later we shall see in detail about various forms of the damage.

Another important parameter used in radiation damage study is the critical dose (D_e). The basic assumption is that the damage is proportional to the energy deposited per unit volume by inelastic scattering similar to the damage caused by x-rays. The critical dose is defined as the electron dose at which effect being observed is reduced to $\left(\frac{1}{e}\right)$ of the initial value. For beam sensitive specimens, it can be observed in terms of disappearing of the diffraction spots. Moreover, the critical dose can be quantified from the Intensity decay of diffraction spots versus the electron dose. The critical dose is known as radiation resistance of the material, and the inverse of it gives us the damage cross section, as determined by the experiment[3].

$$\sigma_d = e/D_e$$

The final goal is to perform the experiment without causing the damage to the specimen. Therefore, it will be good practice to designate temperature, electron dose and the voltage at which the experiment is performed[4].

1.3.2 Types of Radiation Damage

Following figure 2 shows the general types of damage caused due to elastic and inelastic scattering of electrons with the specimen. Later in the section we shall see more details about these types of damage.

Figure 2. Types of damage based on electron scattering

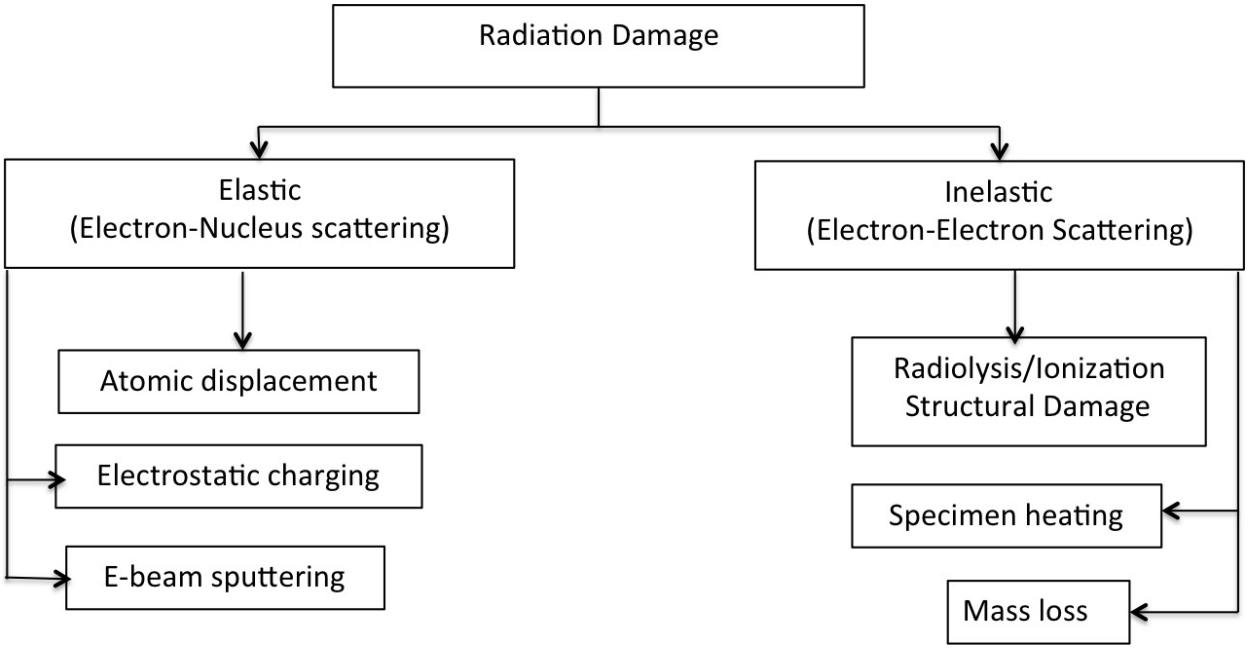

1.3.2.1 Atomic Displacement

The atomic displacement/sputtering damage is very common in metals. During elastic scattering, electrons get displaced by angle θ when they enter the columbic field of the atomic nucleus. In this process, we assume energy and momentum to be conserved. Thus, the amount of energy E transferred can be written as follows

$$E = E_{max} sin^2(\frac{\theta}{2})$$

$$E_{max} = E_0 \left(1.02 + \frac{E_0}{10^6}\right)(465.7A)$$

Here E_0 is the incident energy; E is transferred energy in (eV), and A is mass number of the element. From the equations, we can see that the transfer of energy is high at higher incident

energies, low atomic weight and high angles of scattering. When the value of E exceeds a threshold value E_d, which is dependent on the bond strength, crystal lattice and atomic weights, atomic displacement takes place. When an atom is displaced from the site, it can lead to a combination of vacancy and interstitial also known as Frenkel pairs. Such agglomeration of vacancies can lead to dislocation loops and stacking faults. In TEM to observe the changes, first we need to capture the images of the area before and after irradiation. These vacancy agglomerations can be seen as black-white diffraction contrast in the TEM. The only way to prevent this damage is by using suitable electron dose/ incident energy less than the threshold value[3].

1.3.2.2 Electron-beam Sputtering

Electron-beam sputtering also takes place at high angle elastic scattering at the atom or on the surface of the specimen. The threshold value for sputtering (E_s) is less than the displacement threshold (E_d) because during sputtering the atoms are free to leave the surface than enter an interstitial site. Thus, this could be a problem at 100KeV incident energies also. Thicker specimens don't suffer this damage but for better imaging we need thinner specimens. One way to protect the specimen is by introducing a thin layer of the heavy element at the beam exit surface. The other obvious way is to limit electron dose[3].

1.3.2.3 Specimen heating

Experimental observations of specimen heating are complicated due to various parameters like thermal conductivity, specimen thickness, current, beam size, etc. If the thermal conductivity of the specimen is high, then beam heating is minimum. Mostly beam heating in metals is low whereas for organic specimens like polymers beam heating can lead to thermal degradation or even melting.

It is found that the specimen thickness is independent of the temperature difference. Also, when we decrease the probe size causing an increase in electron density, we find a little increase in the temperature. One of the ways to reduce specimen heating is by using STEM imaging[3].

1.3.2.4 Radiolysis and Mass loss

Organic materials mainly polymers are affected by ionization damage or radiolysis that is caused by inelastic scattering. The damage causes the polymer long chain to break or cross-link to form a new structure. Mainly chemical bonds are broken, and the molecule changes its position leading to loss of crystalline structure for the molecular crystals[5]. Moreover, mass loss also can take place.

The electron-energy loss spectroscopy (EELS) is generated due to inelastic scattering, and it can be very useful in quantitative radiation damage studies. The change in electronic configuration of the molecule can cause loss of fine structure in EELS spectrum. The critical dose (D_e) values can be calculated from the intensity of energy loss-peaks against electron dose[6, 7]. Moreover, by using EELS log-ratio technique we can measure specimen thickness, which will give us a measure of mass loss[8].

For molecular crystals, we can measure critical dose from the fading spots of diffraction patterns as they lose their crystalline structure[9, 10]. In this thesis, we will present a complete procedure on how to do radiation damage study of a polymer and also the show the required analysis to measure the critical dose.

For radiolysis, there is no threshold value below which radiolysis entirely disappears. Cooling the specimen with liquid nitrogen can reduce the structural damage and mass loss. There will not be any decrease in inelastic cross-section, as it doesn't depend on temperature, but it does increase the resistance. Also coating of the specimen with conducting film helps increase the resistance of the specimen to the damage. But the practice of using low imaging dose will be beneficial.

1.3.2.5 Few other Damage mechanisms

The Electrostatic charging can occur for non-conducting specimens. Surface and internal charges can be created. The effect causes the electron beam to deflect. Along with radiolysis, deflection in transmitted beam can cause mechanical distortions for polymeric materials. The

Internal charges create electric fields, and it leads to ion migrations. Electrostatic charging was given as an explanation for the hole drilling in metal-insulator oxides [11]. A Conducting film like carbon can protect the surface, but there is no prevention from internal charges. Moreover, if we use TEM at lower KV, electrostatic charging can be high due to more scattering and beam sensitivity[12].

Another damage can be hydrogen contamination. Over the years, the vacuum has improved in TEM minimizing hydrocarbon content. But the sample can act as a hydrocarbon source. It can pick up hydrocarbons during sample preparations or the transfer of sample through the air. Sometimes such contamination can form dot array pattern, which can be used in lithography for data storage applications[3]. Cooling of the specimen can reduce the movement of hydrocarbons. Also heating or exposing to energetic ions can desorb the hydrocarbons and reduce the damage.

1.3.3 Dose- limited resolution

In X-ray imaging, various synchrotron sources use a technique called X-ray diffraction microscopy (XDM). The method gives nanometer resolution for larger samples, which cannot be used in TEM. The image resolution is limited by the x-ray dose[13]. Similarly in TEM, for radiation sensitive materials like polymers imaging resolution is limited by the electron dosage[12]. We shall see a simple relationship between critical dose and resolution. In TEM, the statistically sufficient number of electrons recorded within each spatial resolution element is

$$N = \delta^2 FD/e$$

where δ is a resolution, F is collection efficiency, the ratio of detected to incident electrons. D is the electron Dose. According to Rose criteria, for an image to be recognizable above the background signal to noise ratio (SNR) should be between 3 and 5. Also, the imaging recorder device has a defective quantum efficiency (DQE), which reduces the SNR by a factor of $(1/2)$. Thus, we can write the dose-limited resolution δ as[6]

$$\delta = (SNR)(DQE)^{-1/2} C^{-1} \left(\frac{FD_e}{e}\right)^{-1/2}$$

Here C is the contrast ratio between adjacent elements and e is the electronic charge. The resolution improves (smaller δ) with the dose as the statistical number of electrons increases, but later the contrast deteriorates leading to decrease in resolution (high δ). Therefore, the best resolution is found at the critical dose (D_e). This is the value, which we are going to determine experimentally in this thesis at electron energies 120KeV and 200KeV. Usually, the dose-limited resolution value for unstrained polymers is near to 5nm[6].

Chapter 2

Materials

2.1 Introduction to Organic Solar cells

Organic electronic materials have a lot of applications towards lightweight, flexible electronics like thin laptops, screens, mobiles, etc. It has a vast amount of applications towards light emitting diodes (OLEDs) and photovoltaics (OPV). These materials have covalent bonding between the atoms. The molecular structures can be crystalline in the range of millimeters, micrometers, and nanometers. Various thermal, optical, electronic properties depend upon the structure of these materials.

Organic semiconductors mainly consist of 90% by mass of hydrocarbons containing carbon, hydrogen, and oxygen. The Crystalline nature of organic semiconductors depends upon the π-conjugation of the polymer backbone i.e. alternating single and double bonds in polymer main chain. The greater the π-conjugation, the higher is the charge transport and crystallinity. Thus, we see here that the crystallinity is an important parameter in the design of organic materials. We can also achieve higher crystallinity with higher molecular weight and having similar molecular weight repeat units i.e. narrower molecular weight distribution.

Solubility is an important aspect of organic semiconductors. For the processing of organic electronics, we need the material to be soluble in common solvents. The addition of side chains to the polymeric backbone improves the solubility of the polymer. Moreover, these side chains do have an impact on the thermal, structure, and electronic property of the polymers. Thus, we have seen the basic design and processing aspects required for efficient functioning of organic materials. Fundamentally organic semiconductors should be able to transport electrons and holes, but practically they can be p-type or n-type materials. Few p-type materials are TIPS-Pentacene[14], Rubrene, etc. The common n-type material is the buckminsterfullerene (C60). A recent review[15] on the progress of molecular crystals for organic photovoltaic (OPV) gives much insight of these materials. Recently 3,6-bis (5-(4-n-butylphenyl) thiophene-2-yl)-2,5-bis (2-ethylhexyl) pyrrolo[3,4-c]pyrrole-1,4-dione, DPP-PR p-type donor material is promising for

OPV applications[16]. In the presented thesis, radiation damage study of this DPP-based polymer is performed.

2.2 Synthesis of OPVs

Initially, planar heterojunctions of donor and acceptor were used for OPVs but had shorter exciton diffusion lengths. Later 3D networking structure of donor and acceptor helped to improve the exciton diffusion length up to 50nm, and the power conversion efficiency (PCE) improved up to 10%. As we have mentioned earlier, the crystallinity/order of materials is very important for the fast charge transport. Moreover, if we can achieve higher order we can get exciton diffusion lengths in the range of micrometers. Thus, synthesis of the single crystalline heterojunctions can prove to be efficient OPVs[16].

The single crystalline heterojunctions were synthesized by vapor phase method[17], but it was difficult to fabricate the device on a small area growth.

The solution grown method[14, 18-20] shows potential for synthesis and fabrication of the single crystalline heterojunctions. The way it is done is by using droplet-pinned crystallization (DPC) method, which we shall discuss for both the individual donor/acceptor organic material and the p-n junction solar cell.

2.2.1 DPC Method

DPC method (figure 3 c) can be used for larger area aligned crystallization of organic crystals[20]. At first the required solution of the material is prepared. Then the solution is put onto a highly doped silicon substrate. The substrate along with droplet is brought onto a hotplate. A pinner (a piece of silicon wafer) is placed on the droplet so that it doesn't slide due to variations in the substrate. Next as the solvent evaporated, crystals start to nucleate near the contact line and grow towards the center of the substrate. The important thing is here we need the alignment of the crystals. This can be achieved by high nuclei density, which will cause mass depletion. Then the crystals will evolve and grow in the preferential direction. Also, steady contact line needs to be maintained.

Large area growth of the crystals can be achieved by patterning the pinners. The smaller the size of the pinners, we can obtain a large fraction of the area of crystals reportedly 100mm wafer area. Moreover, this pinner can be used to position the p and n-channel of organic semiconductors. Such desired patterns will be useful in fabricating complex electronic circuits[20].The DPP-PR single crystals were synthesized [21] and grown by the DPC method explained above. By using the same method we can grow DPP-PR and C_{60} crystal together (figure3b, d) to form a single crystalline heterojunction[16].

Figure 3. (a) DPP-PR structure, (b) DPP-PR-$\boldsymbol{C_{60}}$ OPV, (c, d, e) DPC method for single and two crystals. Images are taken with permission from the references[16, 19, 20].

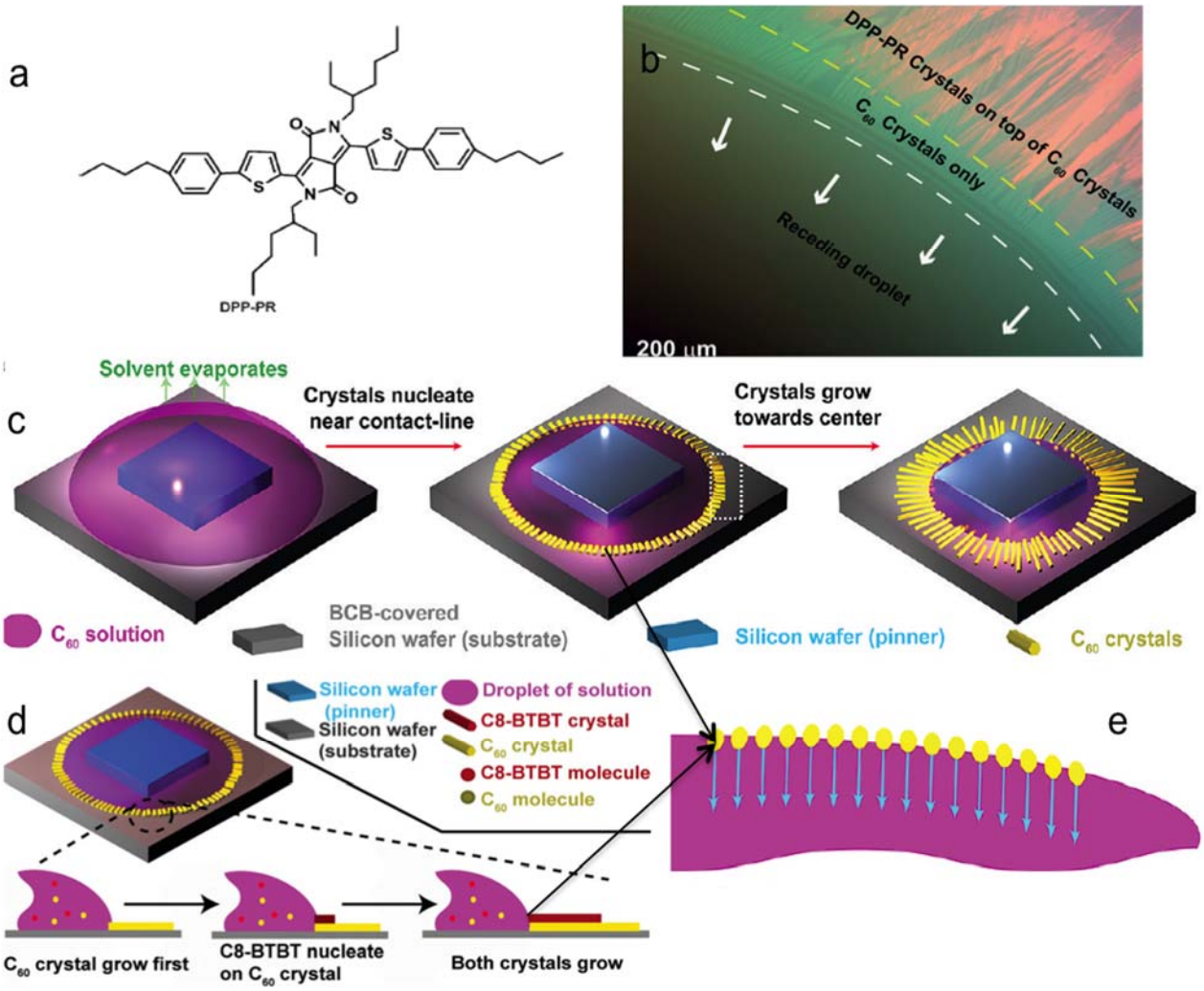

Chapter 3

Experiment and Analysis

3.1 Radiation Damage study of DPP based polymer in JEOL TEM 1400

3.1.1 Experimental Procedure for the set 1 at 120 KeV.

First we shall see the procedure to acquire the diffraction patterns for the polymer DPP-PR. Required steps:

1) Follow basic operational procedure for JEOL TEM 1400.
2) Choose a high tilt holder, which is recommended for beam sensitive specimens.
3) Choose a particular area where you find a good diffraction pattern of the DPP-PR polymer. (Figure 4)
4) Acquire the image of the chosen area along with diffraction aperture, so that it will be useful to calculate the dose rate.
5) Keep taking the diffraction patterns (DP) till you find the all the spots to disappear.
6) Repeat these steps to collect a few sets.

Figure 4. a) Image b) Diffraction Pattern for DPP-PR for set 1 at 120KeV.

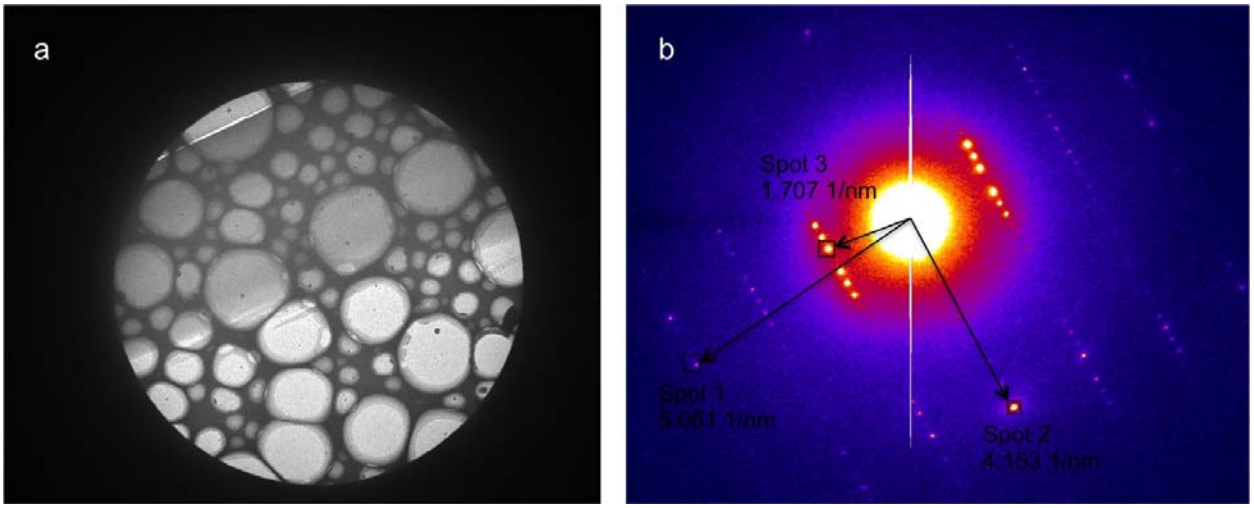

Analysis Procedure Set 1

First we need to calculate the dose rate (DR) value. The formula to calculate the dose rate value is

$$DR = \frac{Mean\ (\ e^{-})}{Exposure\ time(sec) * area(A^{o2})}\ \ (\frac{e^{-}}{A^{o2}.sec})$$

The mean number of electrons can be calculated from ImageJ or Digital Micrograph software. Also the exposure time and area can be found in the image info section.

The dose rate value for set 1 is $DR = 16.79 * 10^{-3}\ (\frac{e^{-}}{A^{o2}.sec})$

The three spots as shown in figure 4b are the chosen spots for the analysis to calculate the critical dose (D_e). These three spots are consistent thought the analysis for the rest of the sets.

Figure 5. Disappearance of the spots in DPs for the set 1. [120KeV]

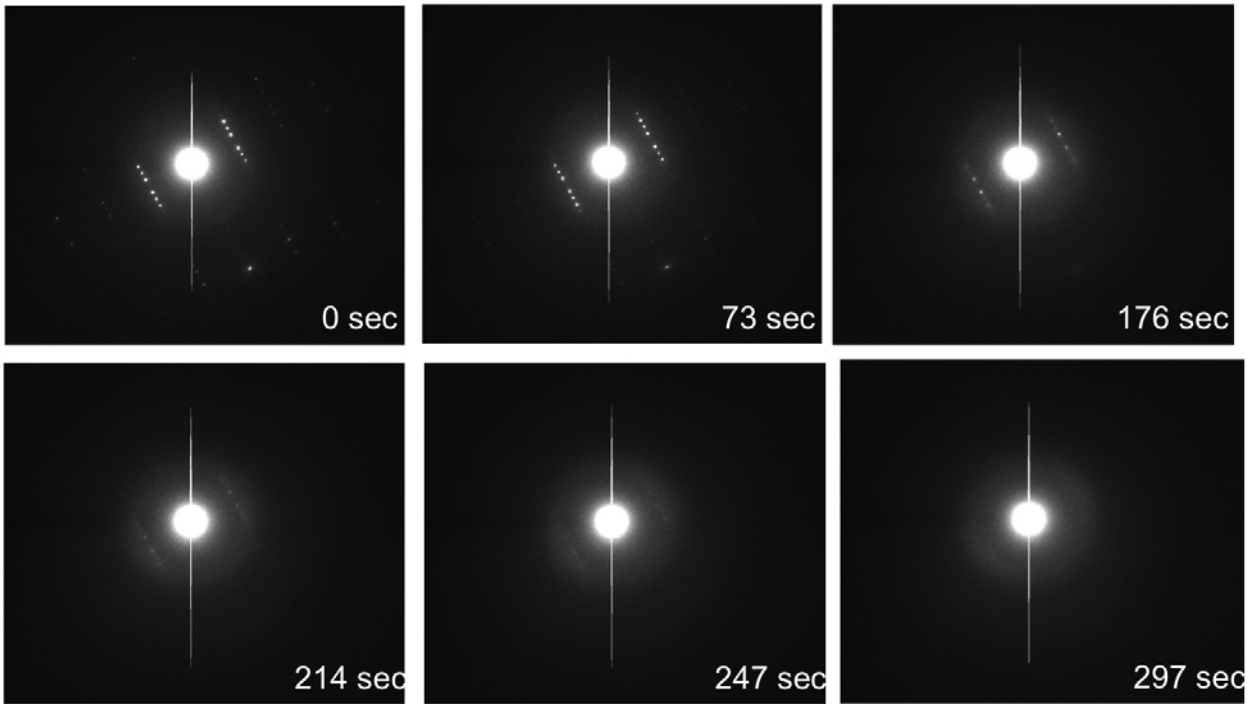

From the above shown figure we calculate the intensity (counts) of the selected spots. The following steps are:

1) Open the ImageJ software.
2) Import the diffraction Patterns to create a stack of images.
3) Align the images in the stack by using a plugin called Template matching. In the plugin the alignment is done using the normalized cross-correlation algorithm.
4) After the images are aligned, select a small rectangle, which would just fit the diffraction spot. Using the Mac command (command M) generate mean intensity value for all the images in the stack. (Table 1)
5) Save the generated table and repeat the process for the required spots.
6) The electron dose is calculated by multiplying the respective time for each DP with the dose rate. Electron Dose (D) $D = T * DR$ $(\frac{e^-}{A^{o2}})$.
7) Repeat the process for the selected spots in the figure4b.

Following the procedure, we generate the table 1 for the spot 1.

Table 1. Showing the intensity values for the respective DPs for the spot 1 [set1, 120KeV].

Mean Intensity (counts)	Time (T) (seconds)	Electron Dose (D) $(\frac{e^-}{A^{o2}})$
8060.854	0	0
6780.561	73	1.22567
5526.013	176	2.95504
5305.905	214	3.59306
5317.767	247	4.14713
5312.741	297	4.98663

Now using table 1 we can generate a plot between Intensity (counts) and electron Dose (D) in the matlab.

Figure 6. Intensity vs. Dose spot 1 [set 1, 120KeV]

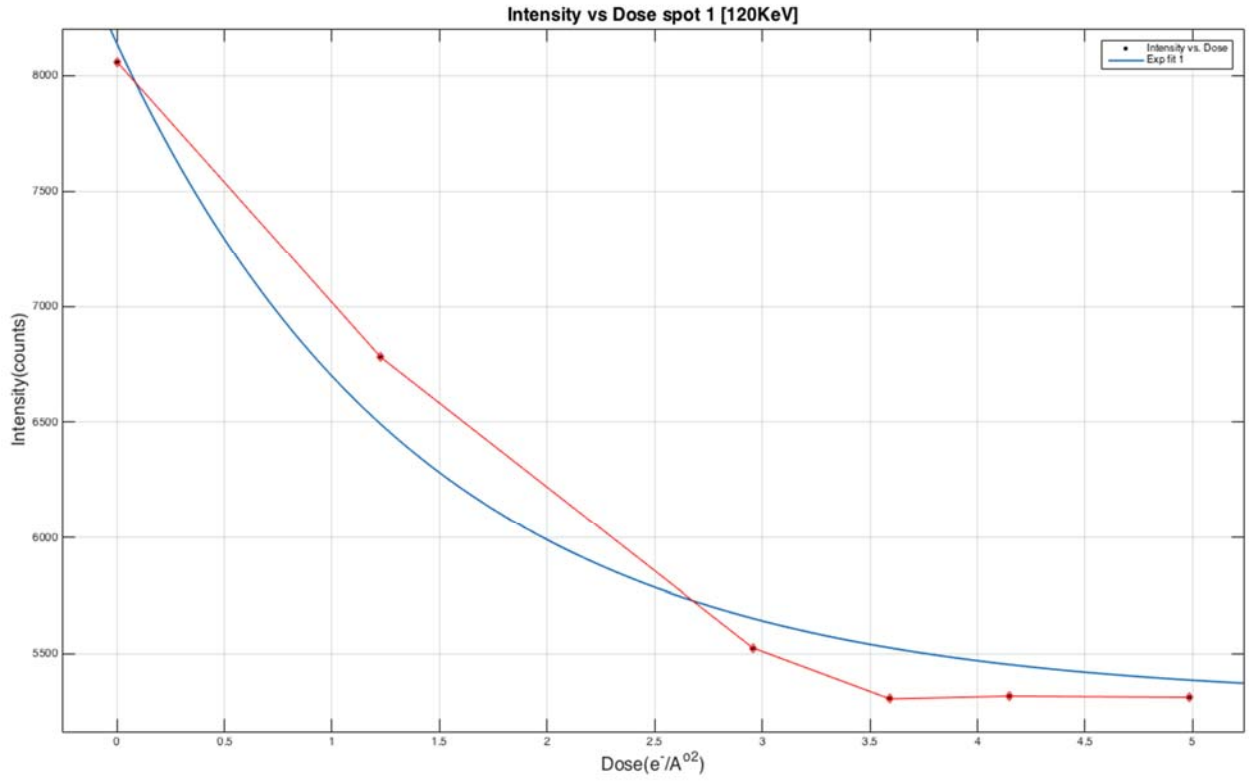

From the matlab exponential fit we get the equation of the curve to be

$$I = 5305 + 2835\ Exp(-0.7102\ D)$$

We know that the critical dose is the value at which the initial intensity decays to (1/e). Hence the above equation is in the form

$$I = A + B\ Exp(-D/D_e)$$

where A, B and D_e can be obtained from the matlab fit curve.

Thus the critical dose comes out to be $D_e = \frac{1}{0.7102} = 1.408\ (\frac{e^-}{A^{o2}})$

Similarly following the analysis procedure above we can obtain the following table 2 and figure7 for spot 2.

Table 2. Showing the Intensity values for the respective DPs for the spot 2 [set 1, 120KeV].

Mean Intensity (counts)	Time (T) (seconds)	Electron Dose (D) ($\frac{e^-}{A^{o2}}$)
20691.4	0	0
14810.454	73	1.22567
8474.6	176	2.95504
7505.694	214	3.59306
7295.383	247	4.14713
6990.463	297	4.98663

Figure 7. Intensity vs. Dose spot 2 [set 1, 120KeV].

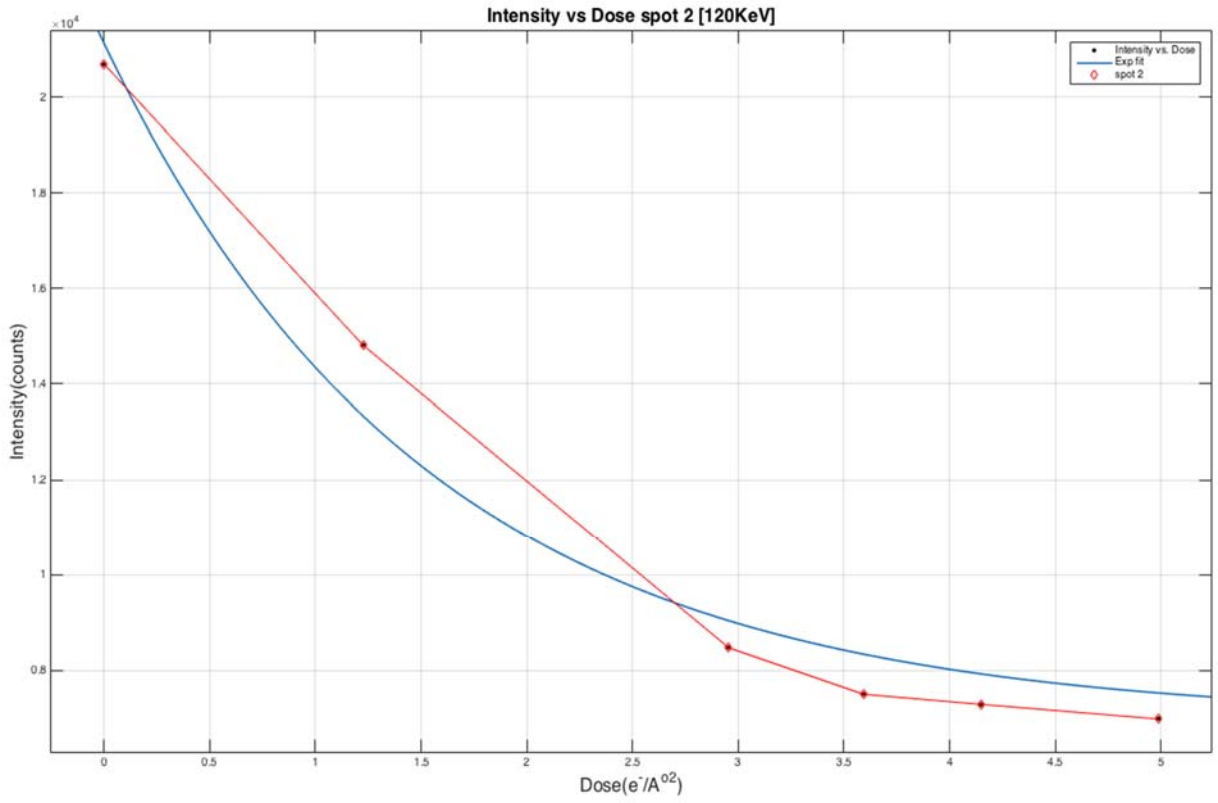

We get the following equation

$$I = 6990 + 1.416 * 10^4 \, Exp(-0.6533D)$$

The critical dose comes out be

$$D_e = \frac{1}{0.6533} = 1.53 \, (\frac{e^-}{A^{o2}})$$

Now we shall do the analysis for the spot 3 following the same procedure.

Table 3. Showing the Intensity values for the respective DPs for the spot 3 [set 1, 120KeV].

Mean Intensity (counts)	Time (T) (seconds)	Electron Dose (D) ($\frac{e^-}{A^{o2}}$)
32009.925	0	0
30764.2	73	1.22567
24138.245	176	2.95504
19692.179	214	3.59306
18339.891	247	4.14713
17120.946	297	4.98663

Figure 8. Intensity vs. Dose spot 3 [set 1, 120KeV]

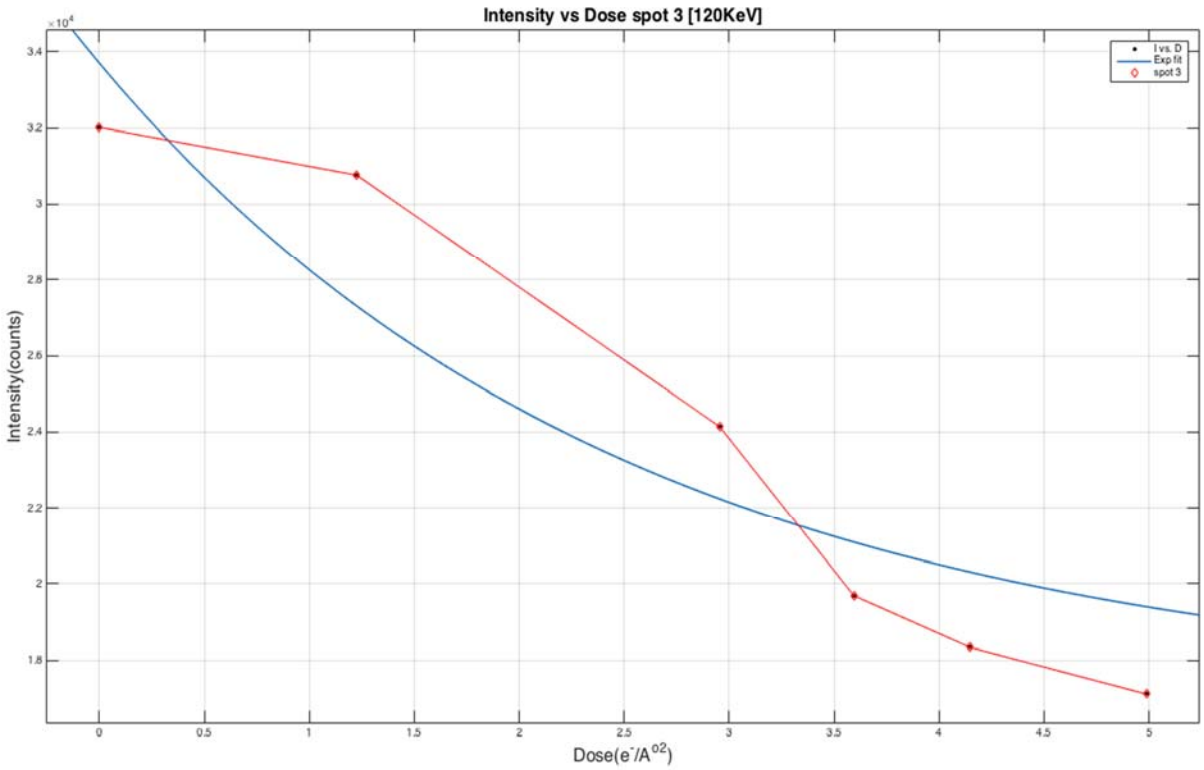

We get the following equation

$$I = 17120 + 1.6 * 10^4 \, Exp(-0.3976D)$$

The critical dose comes out to be

$$D_e = \frac{1}{0.3976} = 2.51 \, (\frac{e^-}{A^{o2}})$$

3.1.2 Experiment and analysis for set 2 at 120 KeV.

For this set, first we will calculate the dose rate value. The value is as shown

$$DR = \frac{Mean\ (e^{-})}{Exposure\ time(sec) * area(A^{o2})} = \frac{330.38}{0.5 * 495.03^{2}} = 2.69 * 10^{-3}(\frac{e^{-}}{A^{o2}.sec})$$

Figure 9. (a) Image of the area (b) Diffraction pattern of DPP-PR with the same selected spots for the set 2 at 120 KeV.

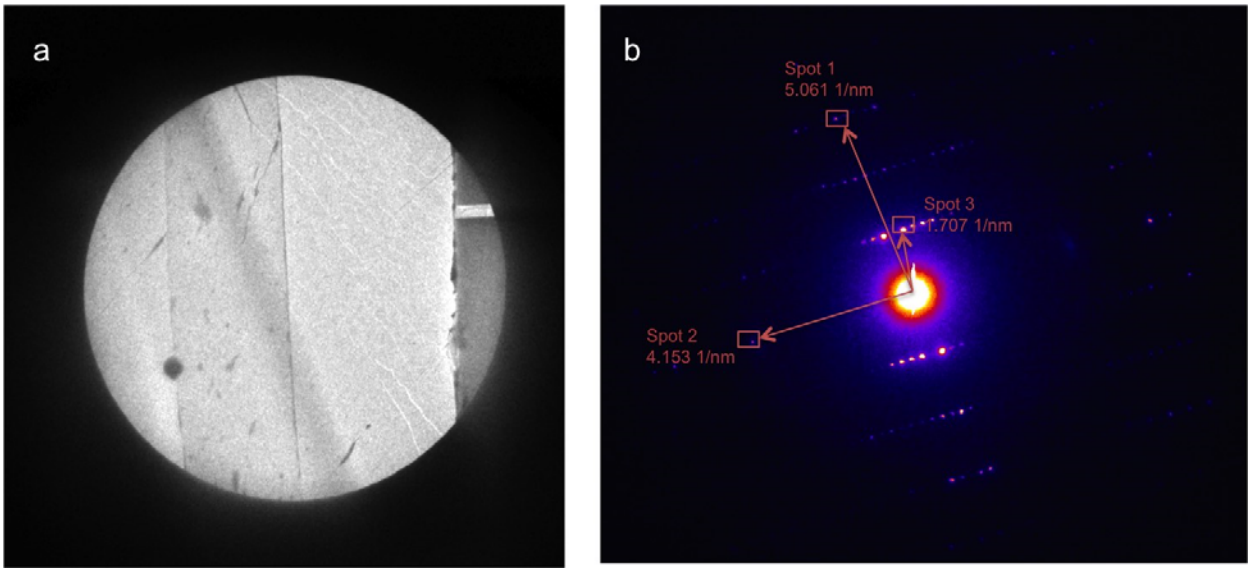

Now the experiment is conducted on the area as explained in the experiment procedure. In this experiment we can see that the dose rate value is less the than the set 1, but its in the same orders of power of ten. This experiment is conducted to understand the dose rate dependency on the critical dose.

Figure 10. Disappearance of the spots in the DPs for the set 2 at 120KeV.

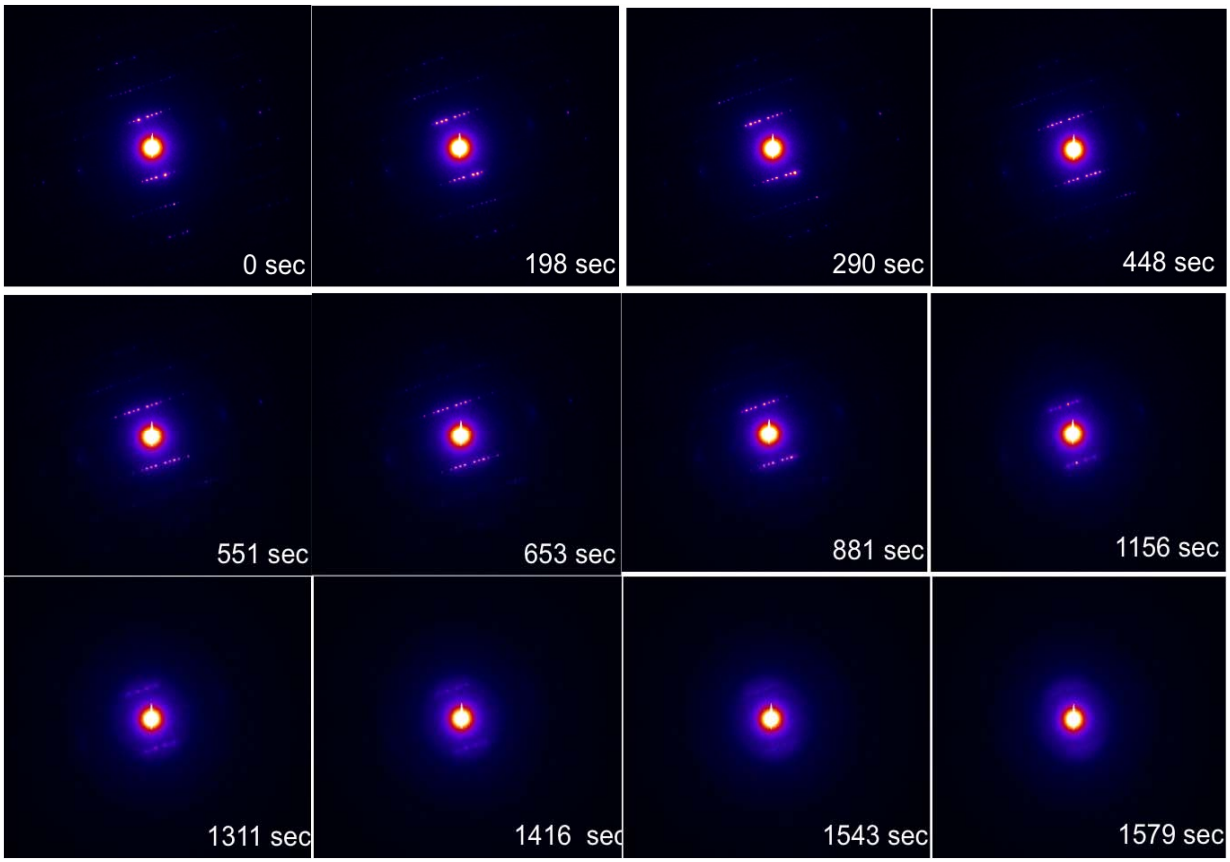

The experiment is conducted till we find the disappearance of the spots as shown in figure 10. We shall follow the same analysis procedure for the selected spots in the set 2.

Analysis for the spot 1 is as follows:

Table 4. Mean Intensity values against the time and electron dose for spot 1 [set 2, 120KeV].

Mean Intensity (counts)	Time (T)(seconds)	Electron Dose (D) ($\frac{e^-}{A^{o2}}$)
3726.94	0	0
2501.554	198	0.53262
2194.393	290	0.7801
2096.821	448	1.20512
1788.571	551	1.48219
1687.53	653	1.75657
1570.696	881	2.36989
1318.024	1156	3.10964
1234.131	1311	3.52659
1244.685	1416	3.80904
1151.994	1543	4.15067
1172.06	1579	4.24751

Figure 11 Intensity vs. Dose spot 1 [set 2, 120KeV].

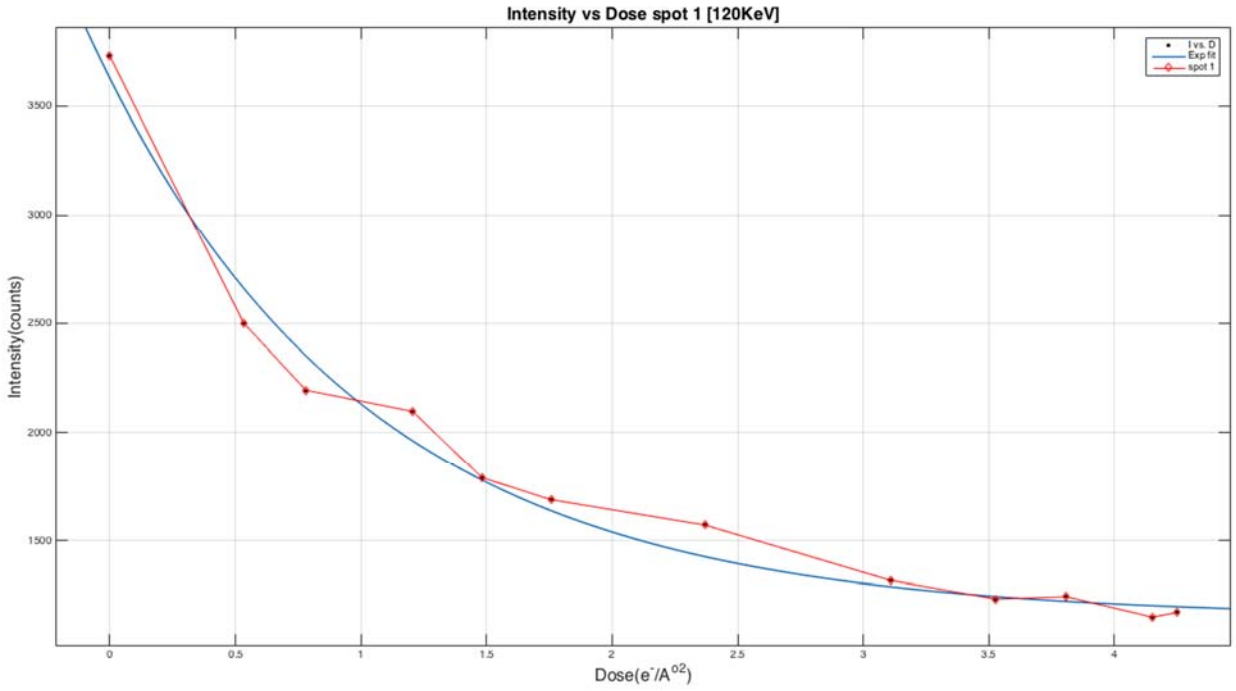

We get the following equation

$$I = 1151 + 2475\ Exp(-0.9265D)$$

The critical dose comes out to be

$$D_e = \frac{1}{0.9265} = 1.01\ (\frac{e^-}{A^{o2}})$$

Next the analysis for spot 2 is as follows:

Table 5. Mean Intensity values against the time and electron dose for spot 2 [set 2, 120KeV].

Mean Intensity (counts)	Time (T) (seconds)	Electron Dose (D) ($\frac{e^-}{A^{o2}}$)
3124.724	0	0
2802.699	198	0.53262
2689.148	290	0.7801
2898.73	448	1.20512
2866.133	551	1.48219
2860.311	653	1.75657
2465.735	881	2.36989
2320.429	1156	3.10964
1910.689	1311	3.52659
1747.781	1416	3.80904
1685.577	1543	4.15067
1627.704	1579	4.24751

Figure 12 Intensity vs. Dose spot 2 [set 2, 120KeV]

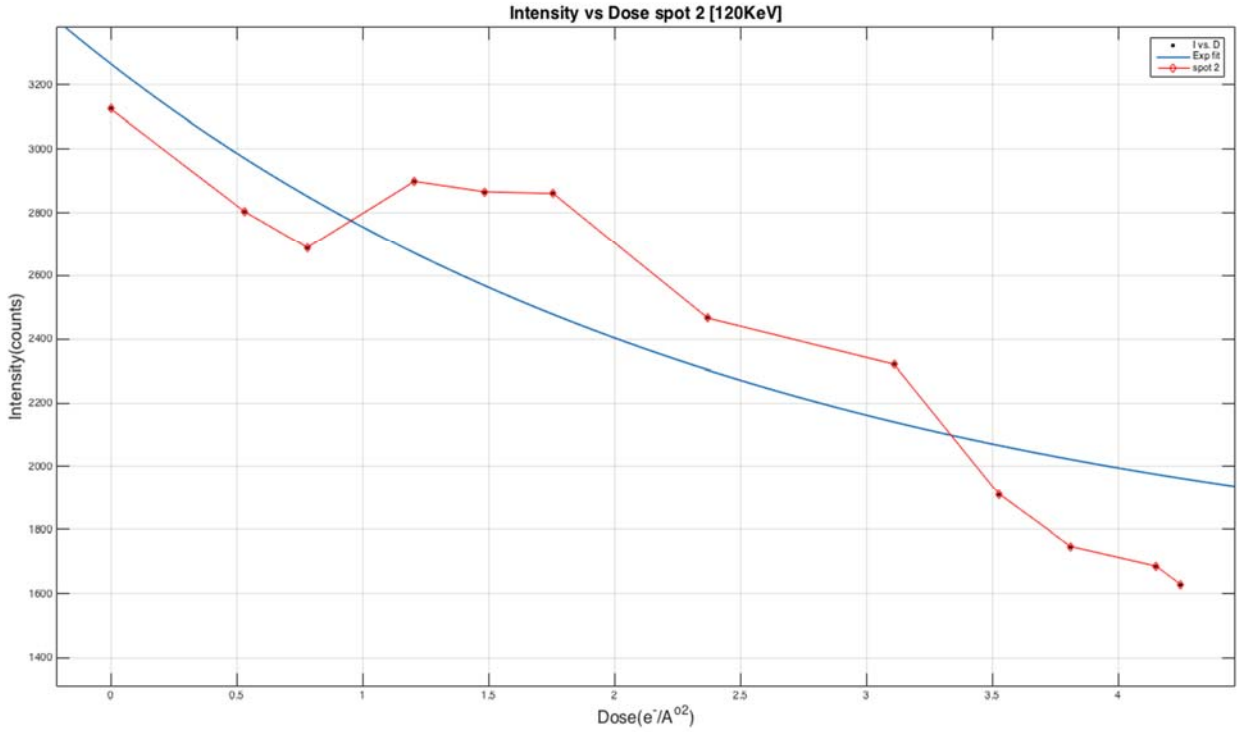

We get the following equation

$$I = 1627.704 + 1638\, Exp(-0.3739D)$$

The critical dose comes out to be

$$D_e = \frac{1}{0.3731} = 2.67\ (\frac{e^-}{A^{o2}})$$

The analysis for the last spot 3 is as follows:

Table 6. Mean Intensity values against the time and electron dose for spot 3 [set 2, 120KeV].

Mean Intensity (counts)	Time (T) (seconds)	Electron Dose D ($\frac{e^-}{A^{o2}}$)
16806.271	0	0
15047.339	198	0.53262
14749.172	290	0.7801
14073.891	448	1.20512
14469.745	551	1.48219
13970.755	653	1.75657
15677.828	881	2.36989
14112.781	1156	3.10964
10545.63	1311	3.52659
9251.083	1416	3.80904
8433.698	1543	4.15067
8305.156	1579	4.24751

Figure 13 Intensity vs. Dose spot 3 [set 2, 120KeV].

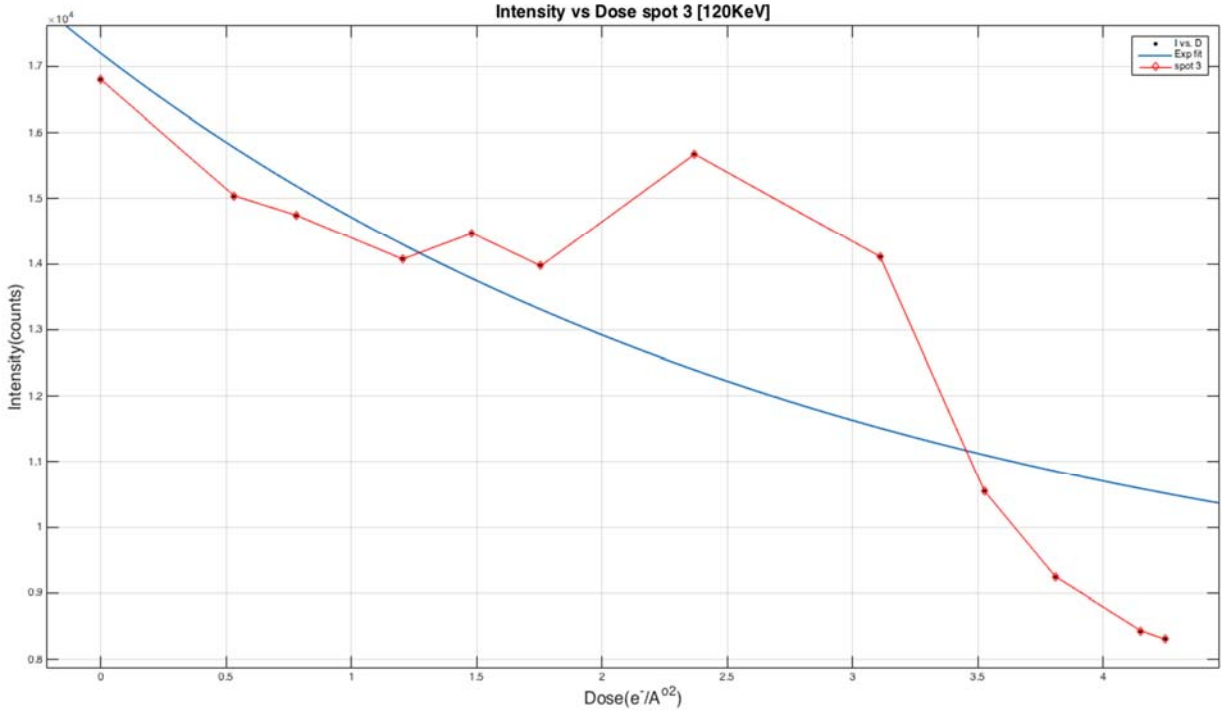

We get the following equation

$$I = 8305.156 + 8898\, Exp(-0.3279D)$$

The critical dose comes out to be

$$D_e = \frac{1}{0.3279} = 3.049\ (\frac{e^-}{A^{o2}})$$

3.1.3 Experiment and analysis for the set 3 at 120 KeV.

For the set 3, the dose rate value is

$$\text{Dose Rate} = 8.47 * 10^{-4}(\frac{e^-}{sec.A^{o2}})$$

The dose rate is kept very low so that it will be useful in understanding the dependency of the dose rate on the critical dose. Following figure 14 shows the area and the selected two spots and figure 15 shows the time series for the disappearance of the selected spots.

Figure 14. (a) Image area (b) Diffraction pattern of DPP-PR with the selected spots fot the set 3 at 120KeV.

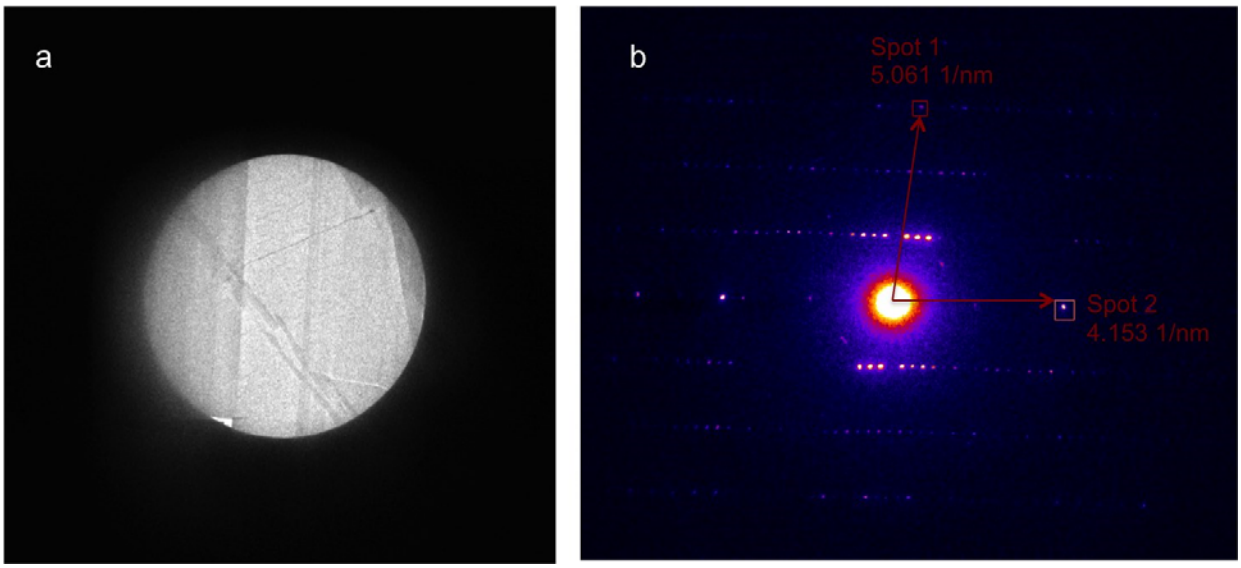

Figure 15. Disappearance of the spots for the set 3 at 120KeV.

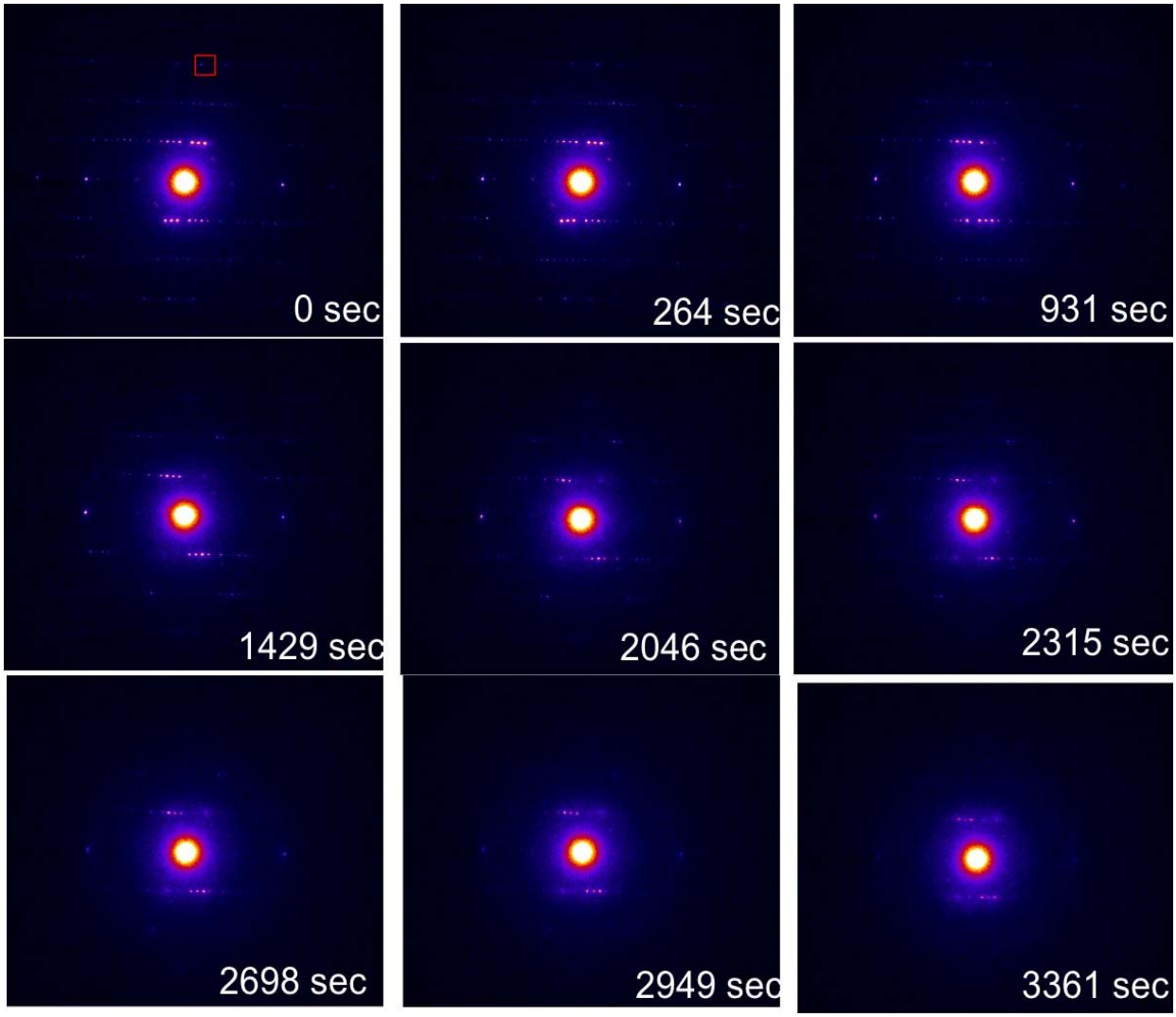

Analysis for the spot 1 as follows:

Table 7. Mean Intensity values against the time and electron dose for spot 1 [set 3, 120KeV].

Mean Intensity (counts)	Time (T) (seconds)	Electron Dose (D)($\frac{e^-}{A^{o2}}$)
2800.734	0	0
3271.008	81	0.068607
2863.461	264	0.223608
2837.656	557	0.471779
2303.699	931	0.788557
2093.855	1069	0.905443
1614.762	1429	1.210363
1746.023	1760	1.49072
1598.301	2046	1.732962
1672.461	2207	1.869329
1670.977	2315	1.960805
1600.551	2549	2.159003
1632.52	2698	2.285206
1643.312	2809	2.379223
1629.801	2949	2.497803
1526.477	3163	2.679061
1663.598	3264	2.764608
1667.859	3361	2.846767

Figure 16. Intensity vs. Dose spot 1 [set 3,120KeV].

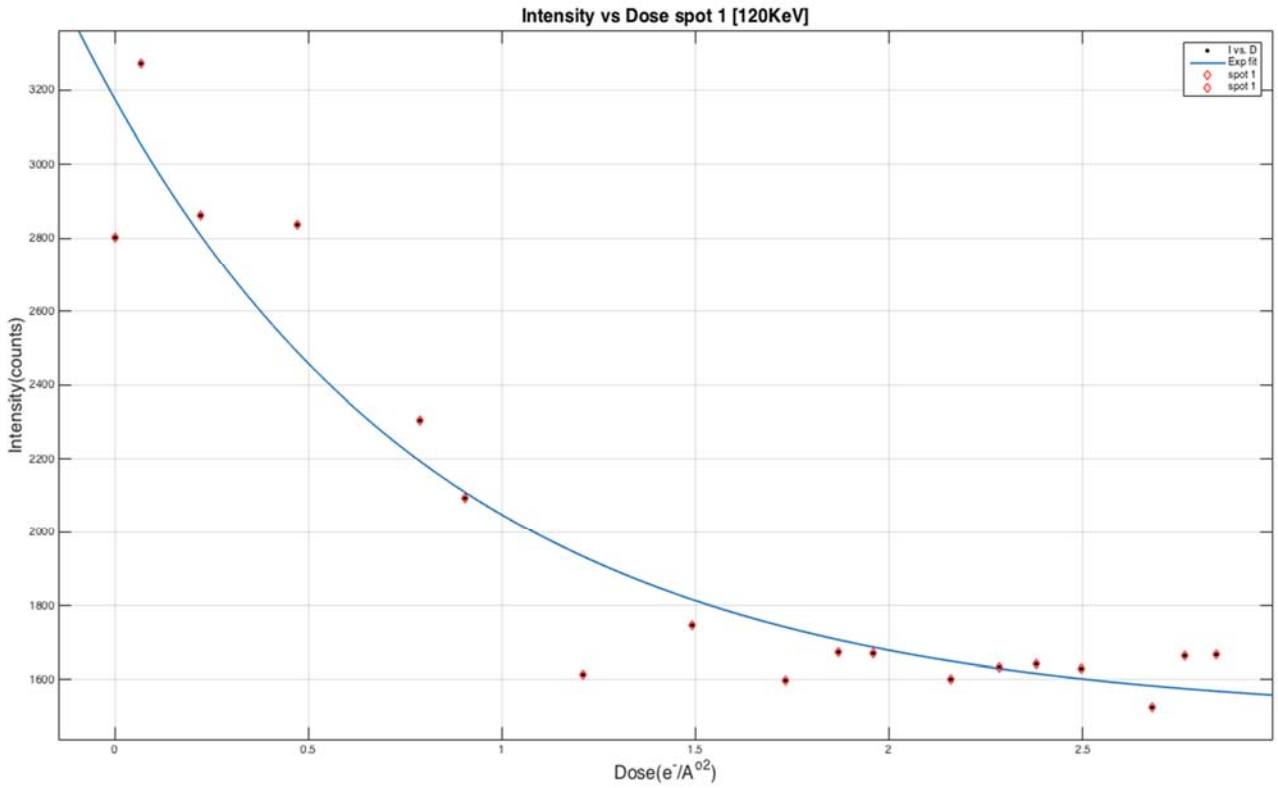

We get the following equation

$$I = 1500 + 1676\, Exp(-1.119D)$$

The critical dose comes out to be

$$D_e = \frac{1}{1.119} = 0.89\ (\frac{e^-}{A^{o\,2}})$$

Analysis of the spot 2 is as follows:

Table 8. Mean Intensity values against the time and electron dose for spot 2 [set 3, 120KeV].

Mean Intensity (counts)	Time (T) (seconds)	Electron Dose (D) ($\frac{e^-}{A^{o2}}$)
6473.875	0	0
6461.988	81	0.068607
6870.462	264	0.223608
6687.069	557	0.471779
6425.512	931	0.788557
5792.144	1069	0.905443
5329.878	1429	1.210363
5753.516	1760	1.49072
5281.309	2046	1.732962
5512.872	2207	1.869329
5773.497	2315	1.960805
4947.028	2549	2.159003
4665.072	2698	2.285206
4238.888	2809	2.379223
3939.212	2949	2.497803
3406.003	3163	2.679061
3405.794	3264	2.764608
3218.194	3361	2.846767

Figure 17. Intensity vs. Dose spot 2 [set 3, 120 KeV].

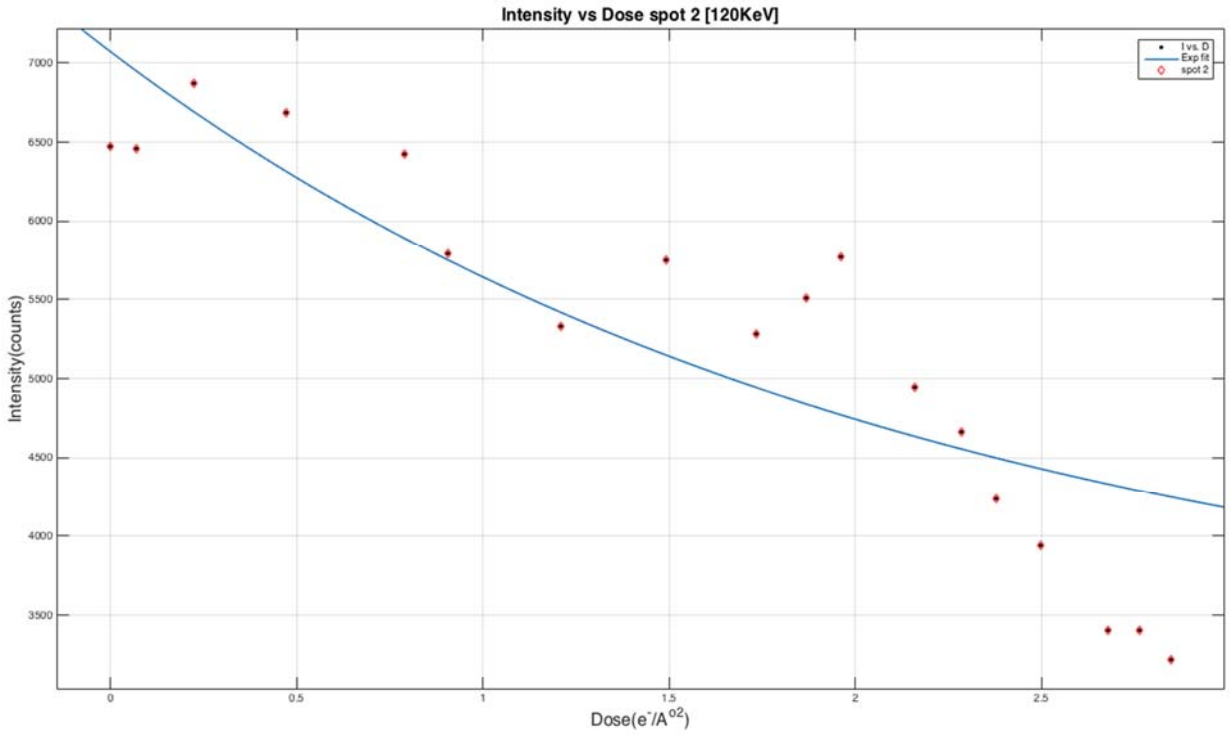

We get the following equation

$$I = 3218.194 + 3854\, Exp(-0.4633D)$$

The critical dose comes out to be

$$D_e = \frac{1}{0.4633} = 2.15\ \left(\frac{e^-}{A^{o2}}\right)$$

3.1.4 Conclusions from the work on JEOL 1400

From the sets 1, 2 and 3, we can see that though the dose rate values are different, the critical dose values do not alter much for each of the selected spots. Thus, we can conclude that the critical dose doesn't depend upon the dose rate. We conducted similar experiments to get statistical significance on the critical dose value. The critical dose value for spot 3 can be approximated as ≈ 3 $(\frac{e^-}{A^{o2}})$. Therefore for this polymer (DPP-PR) the critical dose value at 120KeV is approximately 3 $(\frac{e^-}{A^{o2}})$.

Table 9. Critical Dose values for all the sets taken at 120KeV for the selected spots.

Critical Dose Values $D_e(\frac{e^-}{A^{o2}})$	Spot 1 5.061 1/nm	Spot 2 4.153 1/nm	Spot 3 1.707 1/nm
Set 1 DR=$16.79 * 10^{-3}$ $(\frac{e^-}{A^{o2}.sec})$	1.48	1.53	2.51
Set 2 DR=$2.69 * 10^{-3}$ $(\frac{e^-}{A^{o2}.sec})$	1.01	2.67	3.04
Set 3 DR= $8.47 * 10^{-4}$ $(\frac{e^-}{A^{o2}.sec})$	0.89	2.15	
Set 4 DR= $5.68* 10^{-3}$ $(\frac{e^-}{A^{o2}.sec})$	1.55	2.65	3.09
Set 5 DR= $2.76*10^{-3}(\frac{e^-}{A^{o2}.sec})$	1.00	2.20	1.69
Set 6 DR= $2.65*10^{-3}(\frac{e^-}{A^{o2}.sec})$	0.5	0.98	1.66

3.2 Radiation damage study of DPP based polymer in JEOL TEM 2100F

We are interested in knowing what happens to critical dose values at higher electron energies. Thus, we are now going to perform similar radiation damage study of the DPP polymer at higher electron energy of 200KeV. In the following experiment and analysis, we calculate the critical dose values for the same three spots that were chosen in the previous experiment at 120KeV. The dose rate value is maintained low and constant, which can be achieved at the spot size 5 in the JEOL 2100F.

3.2.1. Experiment and analysis for the set 1 at 200KeV.

For all the sets taken at 200KeV the dose rate value is kept constant. The value of dose rate is

$$DR = 4.97 * 10^{-2} \frac{e^-}{A^{o2}.sec}$$

The experiment and analysis procedure is similar to the JEOL 1400. The following figure18 shows the area and diffraction pattern for the set 1. Figure 19 shows a time series for the disappearance of the spots.

Figure 18. (a) Image (b) Diffraction Pattern with spots taken for the set 1 at 200KeV.

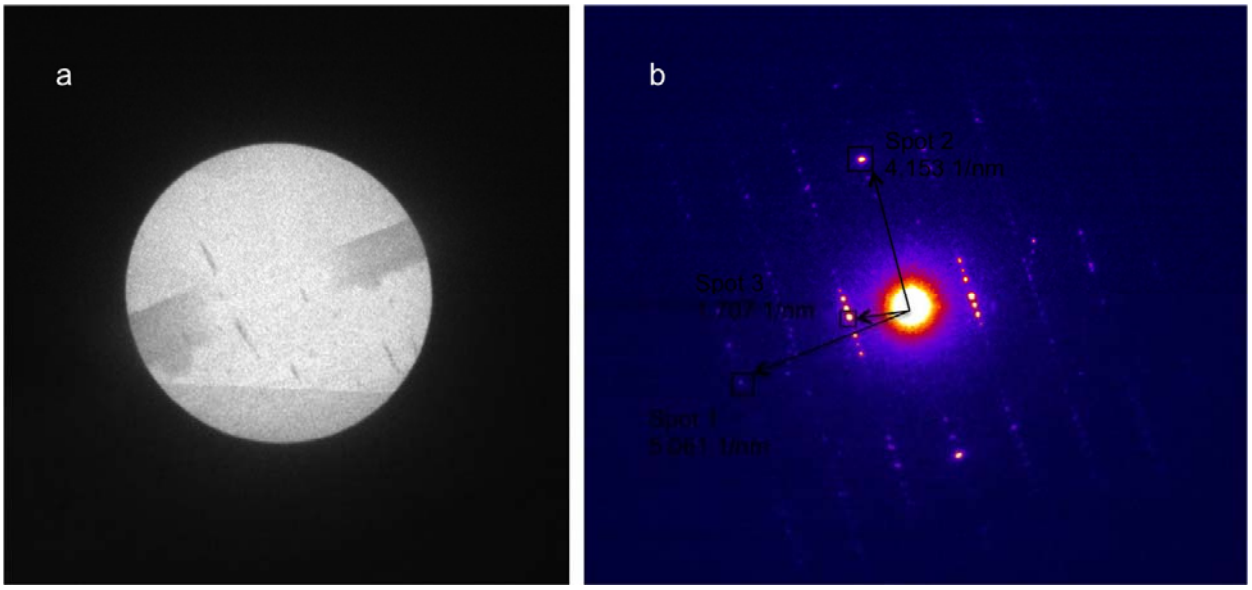

Figure 19. Disappearance of the spots in the DPs for the set 1 at 200KeV

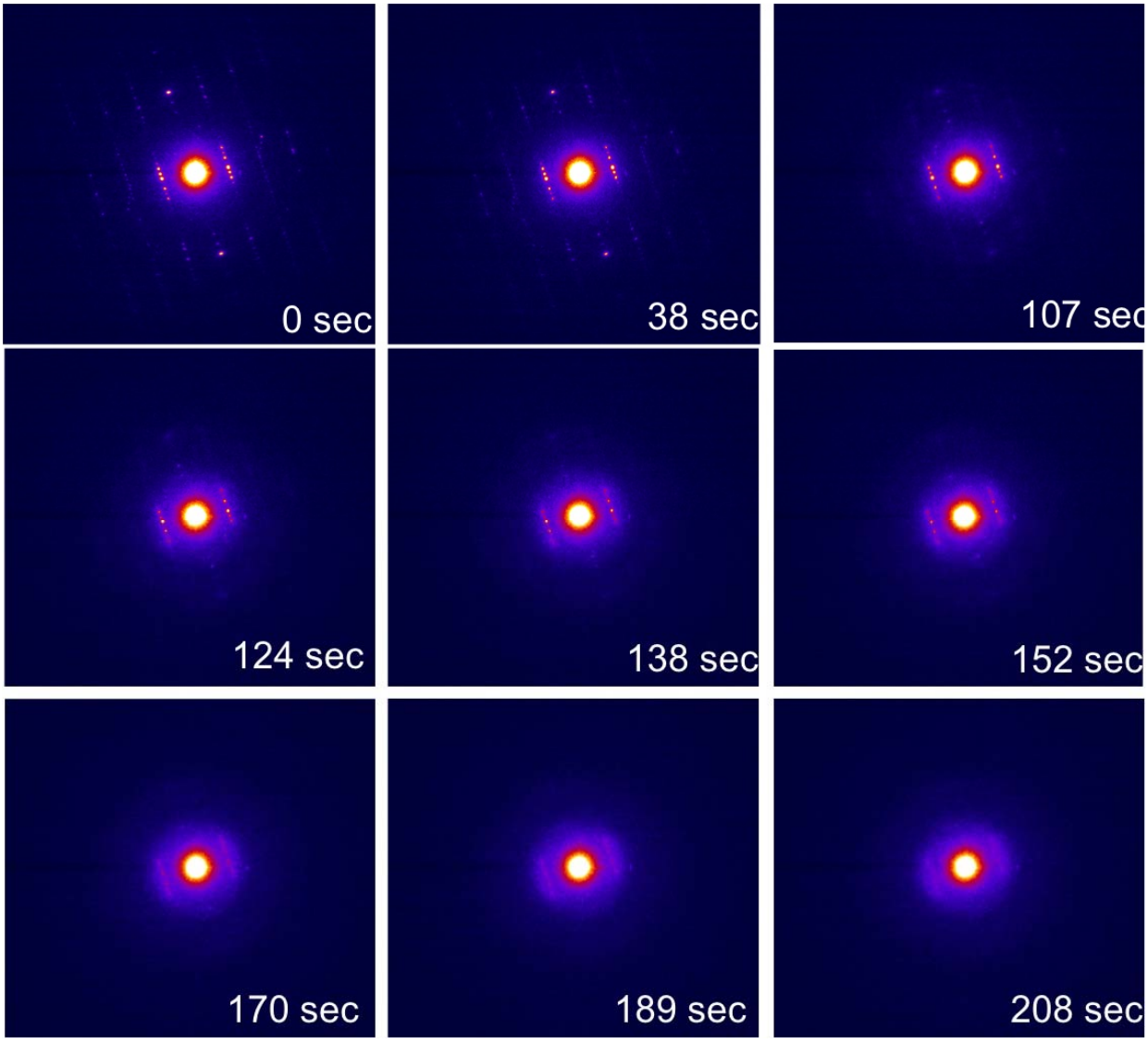

Analysis for the spot 1 as follows:

Table 10. Mean Intensity values against the time and electron dose for spot 1 [set 1, 200KeV].

Mean Intensity (Counts)	Time (seconds)	Electron Dose (D)($\frac{e^-}{A^{o2}}$)
5169	0	0
4918.75	14	0.6958
5093.772	38	1.8886
4720.986	75	3.7275
4539.557	107	5.3179
4277.147	124	6.1628
4129.625	138	6.8586
4002.611	152	7.5544
4132.515	170	8.449
3887.741	189	9.3933
3889	208	10.3376

Figure 20. Intensity vs. Dose spot 1 [set1, 200KeV]

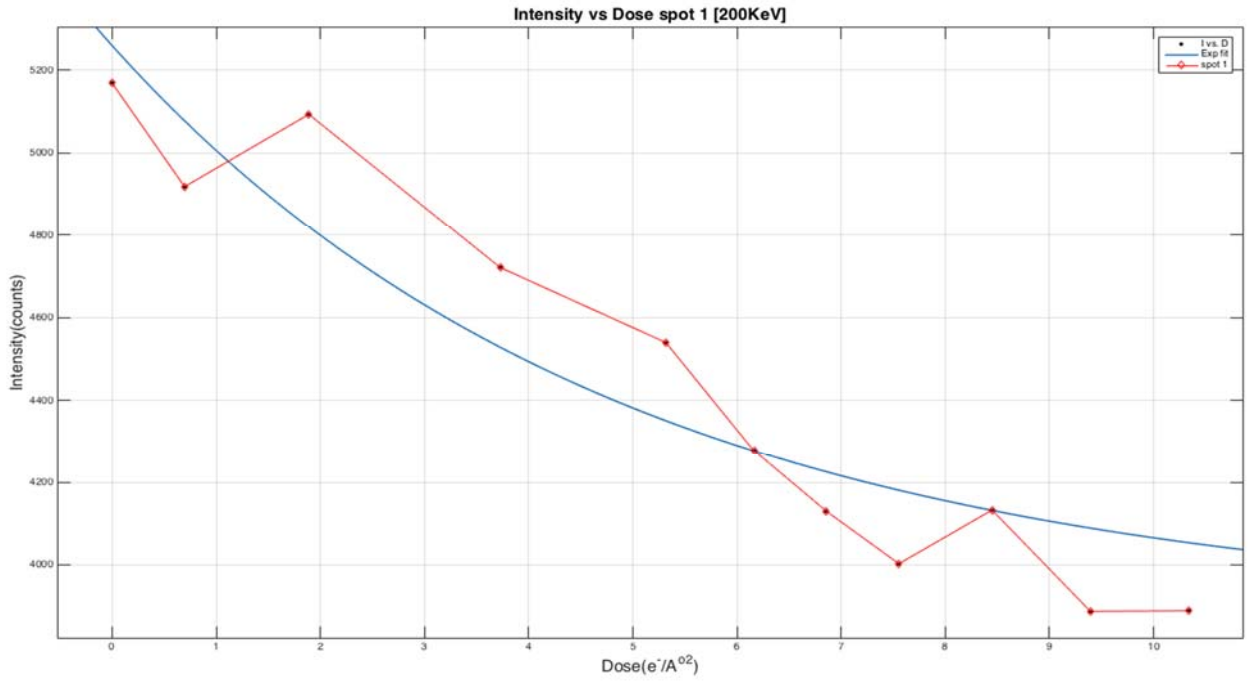

We get the following equation

$$I = 3887.74 + 1372\ Exp(-0.2044D)$$

The critical dose comes out to be

$$D_e = \frac{1}{0.2044} = 4.89\ \left(\frac{e^-}{A^{o2}}\right)$$

Analysis for the spot 2:

Table 11. Mean Intensity values against the time and electron dose for spot 2 [set 1, 200KeV]

Mean Intensity (counts)	Time (seconds)	Electron Dose (D)($\frac{e^-}{A^{o2}}$)
19847.949	0	0
16989.245	14	0.6958
15181.658	38	1.8886
13309.747	75	3.7275
7075.272	107	5.3179
6146.333	124	6.1628
5717.664	138	6.8586
5190.802	152	7.5544
4996.027	170	8.449
5002.002	189	9.3933
4639.725	208	10.3376

Figure 21. Intensity vs. Dose spot 2 [set1, 200KeV].

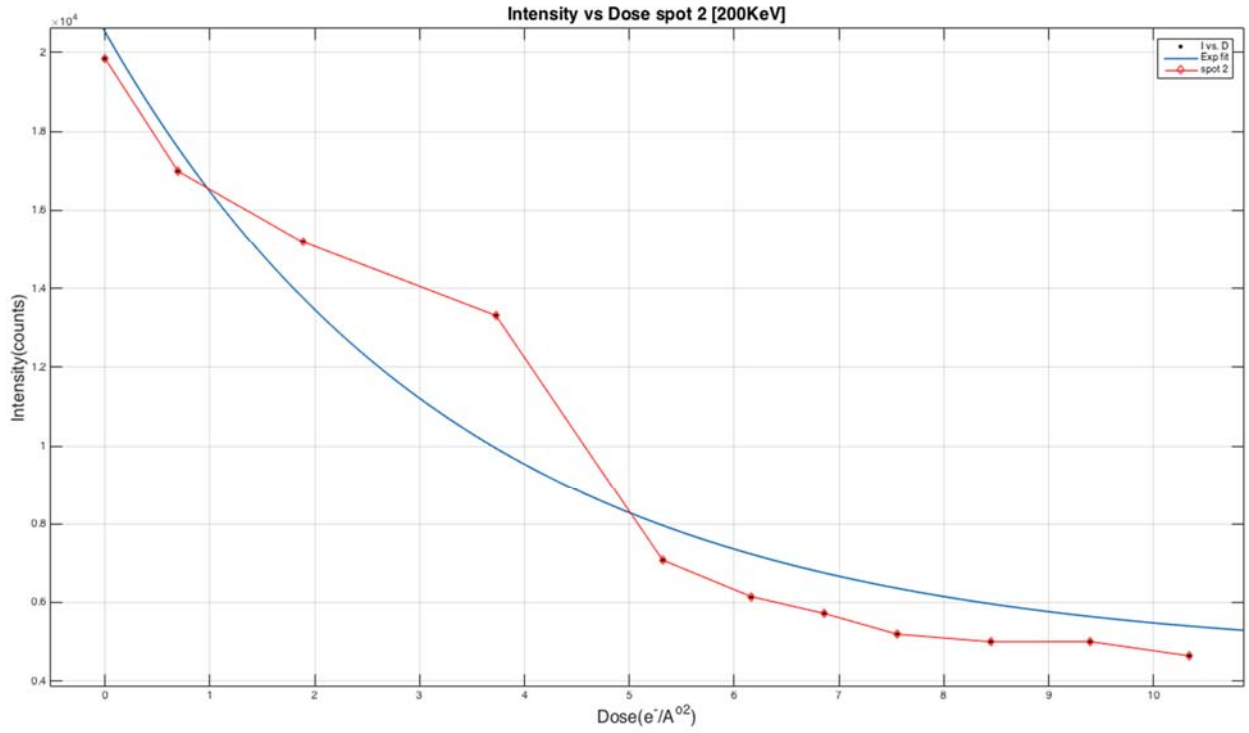

We get the following equation

$$I = 4639.7 + 1.58 * 10^4 \, Exp(-0.2943D)$$

The critical dose comes out to be

$$D_e = \frac{1}{0.2943} = 3.39 \left(\frac{e^-}{A^{o2}}\right)$$

Analysis for the spot 3:

Table 12. Mean Intensity values against the time and electron dose for spot 3 [set 1, 200KeV].

Mean Intensity (counts)	Time (seconds)	Electron Dose (D)($\frac{e^-}{A^{o2}}$)
30324.839	0	0
31515.565	14	0.6958
31987.907	38	1.8886
32250.5	75	3.7275
30269.373	107	5.3179
27896.518	124	6.1628
23688.637	138	6.8586
19562.692	152	7.5544
16335.02	170	8.449
14965.798	189	9.3933
13655.812	208	10.3376

Figure 22. Intensity vs. Dose spot 3 [set1, 200KeV]

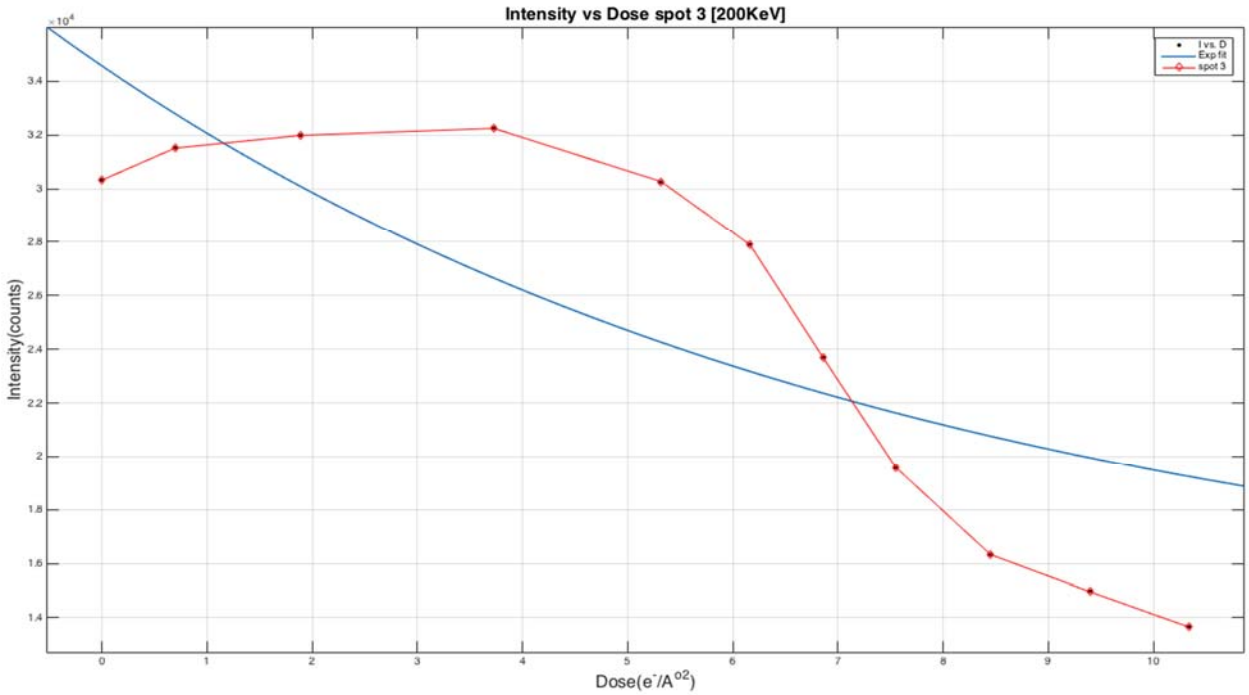

We get the following equation

$$I = 13655.81 + 2.092 * 10^4 \, Exp(-0.1278D)$$

The critical dose comes out to be

$$D_e = \frac{1}{0.1278} = 7.87 \left(\frac{e^-}{A^{o2}}\right)$$

3.2.2. Experiment and analysis for the set 2 at 200KeV.

We present another set at the same dose rate value. Following figure23 shows the area and diffraction pattern. Figure 24 represents the time series over which the spots disappear. Similar analysis for the three spots is shown in the section.

Figure 23. (a) Image (b) Diffraction Pattern with spots taken for set 2 at 200KeV

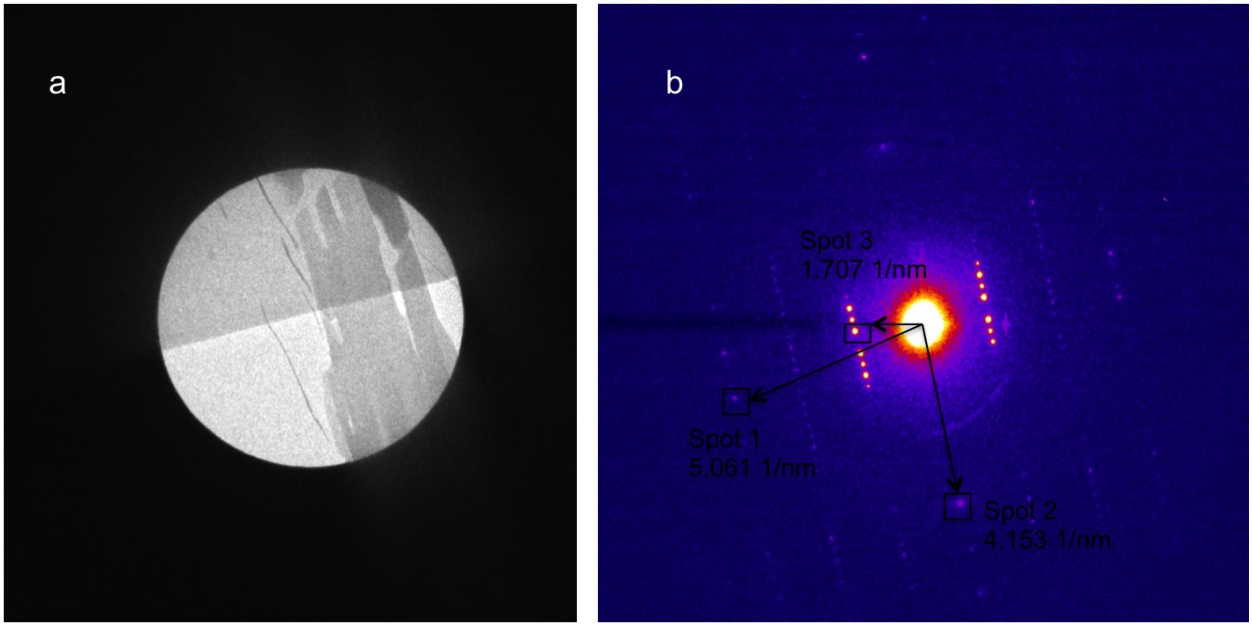

Figure 24. Disappearance of the spots in the DPs for the set 2 at 200KeV

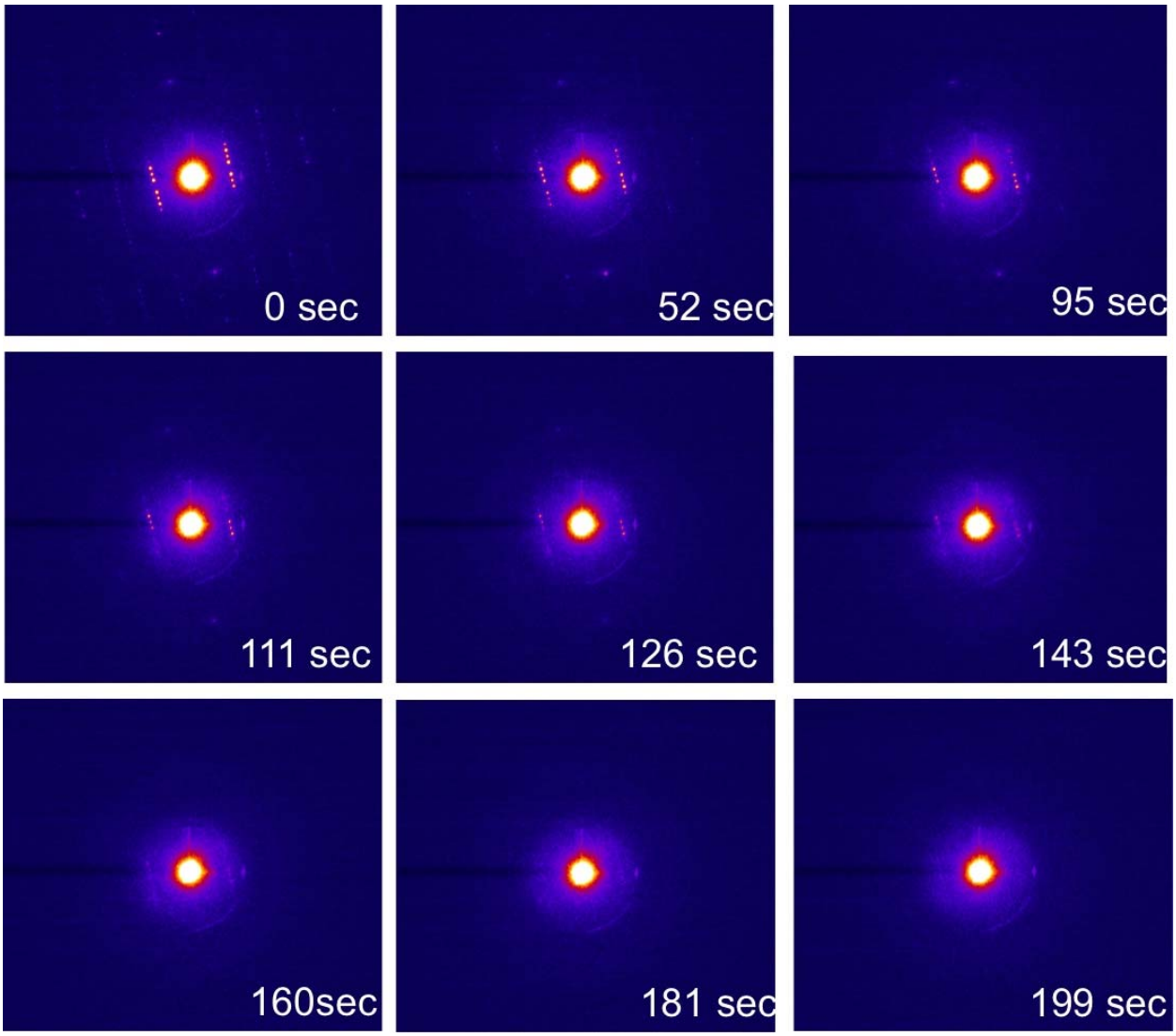

Analysis for the spot 1:

Table 13. Mean Intensity values against the time and electron dose for spot 1 [set 2, 200KeV]

Mean Intensity (counts)	Time (seconds)	Electron Dose (D)($\frac{e^-}{A^{o2}}$)
7016.365	0	0
6227.052	26	1.2922
5732.027	52	2.5844
5597.213	66	3.2802
5344.959	81	4.0257
5337.721	95	4.7215
5425.392	111	5.5167
5131.145	126	6.2622
5002.163	143	7.1071
5210.138	160	7.952
5091.288	181	8.9957
5131.143	199	9.8903

Figure 25. Intensity vs. Dose spot 1 [set 2, 200KeV].

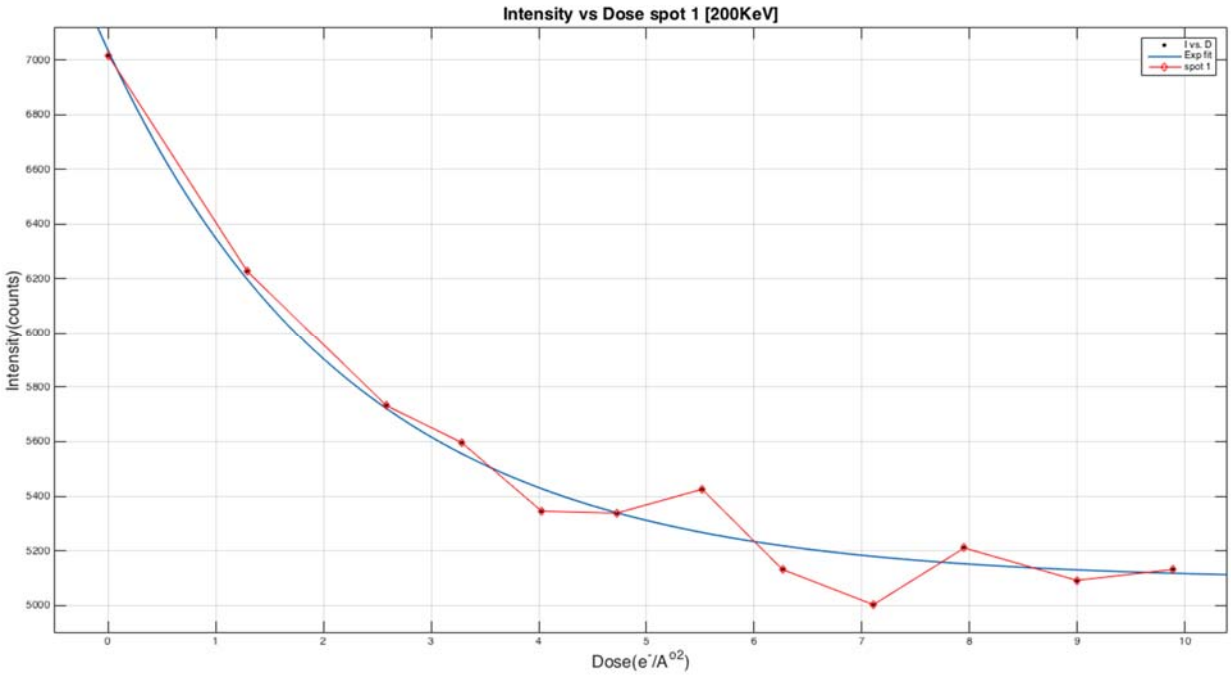

We get the following equation

$$I = 5091.288 + 1942\ Exp(-0.4357D)$$

The critical dose comes out to be

$$D_e = \frac{1}{0.4357} = 2.295\ \left(\frac{e^-}{A^{o2}}\right)$$

Analysis for the spot 2:

Table 14. Mean Intensity values against the time and electron dose for spot 2 [set 2, 200KeV].

Mean Intensity (counts)	Time (seconds)	Electron Dose (D) $(\frac{e^-}{A^{o2}})$
8999.667	0	0
8419.578	26	1.2922
9698.612	52	2.5844
9628.005	66	3.2802
8620.861	81	4.0257
7684.303	95	4.7215
6845.923	111	5.5167
6676.704	126	6.2622
5897.086	143	7.1071
5862.886	160	7.952
5650.676	181	8.9957
5401.613	199	9.8903

Figure 26. Intensity vs. Dose spot 2 [set 2, 200KeV].

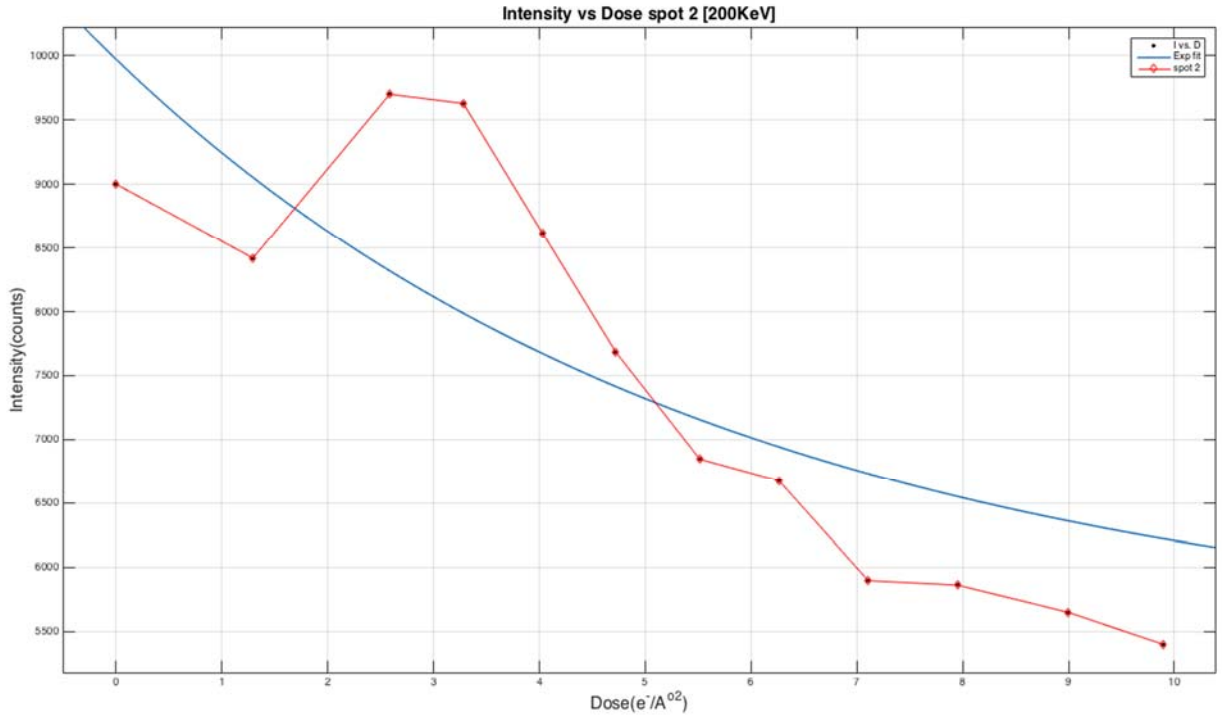

We get the following equation

$$I = 5401.61 + 4569\ Exp(-0.1735D)$$

The critical dose comes out to be

$$D_e = \frac{1}{0.1735} = 5.76\ \left(\frac{e^-}{A^{o2}}\right)$$

Analysis for the spot 3:

Table 15. Mean Intensity values against the time and electron dose for spot 3 [set 2, 200KeV].

Mean Intensity (counts)	Time (seconds)	Electron Dose (D) ($\frac{e^-}{A^{o2}}$)
26511.561	0	0
24225.725	26	1.2922
21259.222	52	2.5844
20098.167	66	3.2802
18018.751	81	4.0257
17739.683	95	4.7215
16023.886	111	5.5167
13083.646	126	6.2622
11654.558	143	7.1071
10929.005	160	7.952
10181.474	181	8.9957
10463.958	199	9.8903

Figure 27. Intensity vs. Dose spot 3 [set 2, 200KeV].

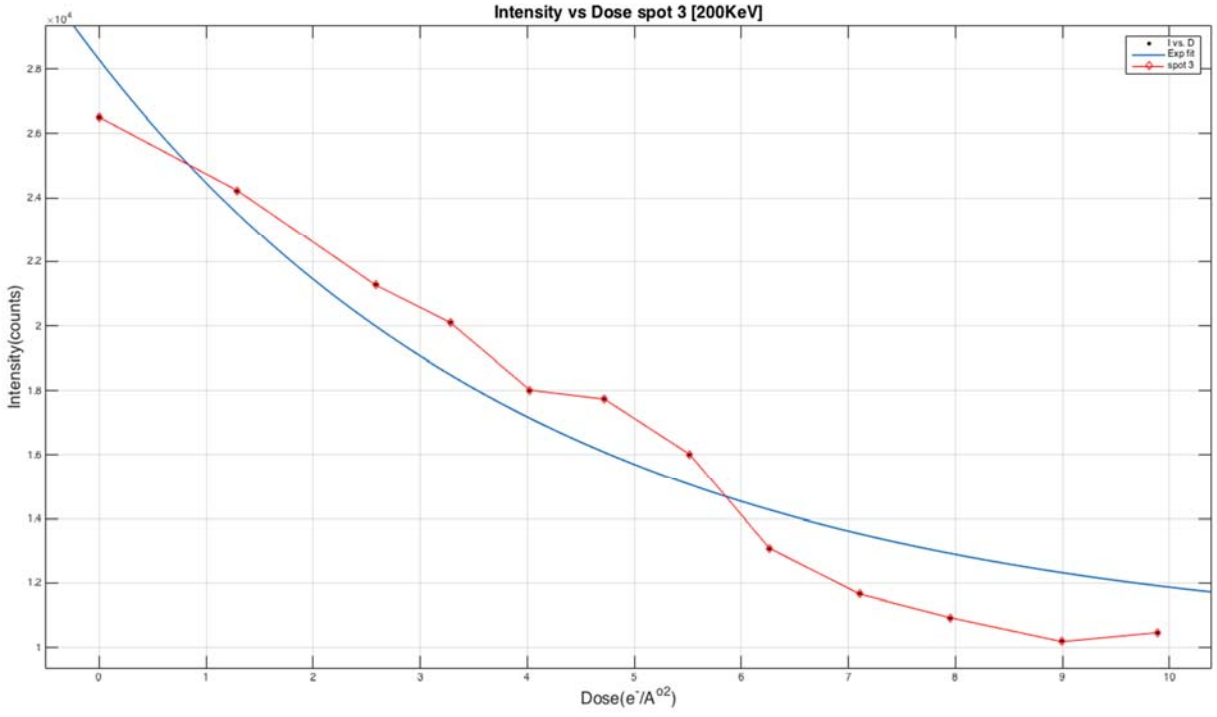

We get the following equation

$$I = 10181.47 + 1.811 * 10^4\, Exp(-0.2374D)$$

The critical dose comes out to be

$$D_e = \frac{1}{0.2374} = 4.21\ \left(\frac{e^-}{A^{o2}}\right)$$

3.2.3. Conclusions from the work on JEOL 2100F.

Similar to set 1 and set 2, we acquired data from various sets for the three spots at 200KeV and tabulated as follows.

Table 16. Critical Dose values for all the sets on JEOL 2100F

Critical Dose Values $D_e(\frac{e^-}{A^{o2}})$	Spot 1 5.061 1/nm	Spot 2 4.153 1/nm	Spot 3 1.707 1/nm
Set 1	4.89	3.39	7.87
Set 2	2.295	5.76	4.21
Set 3	4.81		7.51
Set 4	4.78		5.70
Set 5	3.67		3.87
Set 6		3.23	
Set 7		3.235	
Set 8		2.19	

From the table 16 we can observe that the critical dose values for the same material DPP has increased at 200KeV. From the spot 3 critical dose values, we can approximate the critical dose value for the DPP at 200KeV approximately as $D_e \approx 6\ (\frac{e^-}{A^{o2}})$. Later in the conclusions section we shall see the implementations of these results.

3.3 Calibration of the Diffraction Pattern on JEOL 1400.

Here we are going to present how to calibrate the Diffraction Patterns so as to get the proper values of the reciprocal space k and the d-spacing.

Procedure:

1) Take a standard gold (Au) sample and get a diffraction pattern as shown in figure 28a. The DP is taken at 300mm camera length.
2) Take the diffraction pattern of the desired sample at the same camera length.
3) Calculate the d-spacing values for an Au FCC crystal structure, which can also be found in an International Center for Diffraction Data (ICDD) card. For a cubic system
$$d = \frac{a}{\sqrt{h^2 + k^2 + l^2}}$$
where a = 0.4079 nm is the lattice constant for Au, (hkl) are the Miller Indices.
4) Next, the k values can be calculated as k=1/d.
5) Using digital micrograph measure the radius of the ring of the diffraction pattern. This radius gives us the k value. If the calculated and experimental k values are different, we need to scale the calibration.
6) This new calibration scale is substituted for the properties of the image for a particular camera length. Thus, we get the proper k values for the measured spots on the diffraction pattern.
7) For this particular set 1 at 120KeV for camera length 300mm, calibration scale can be found by
$$Calibration\ scale = \ default\ calibration\ scale * \frac{Calculaed\ k}{k\ determined\ from\ the\ ring\ DP}$$

This formula is general for all the cases. If the determined k value is found smaller than the calculated value, then the new calibration scale will be larger than the default and vice versa.

Figure 28. a) Au (FCC) standard diffraction Pattern. (b) DP of set 1 at 120 KeV for camera length 300mm.

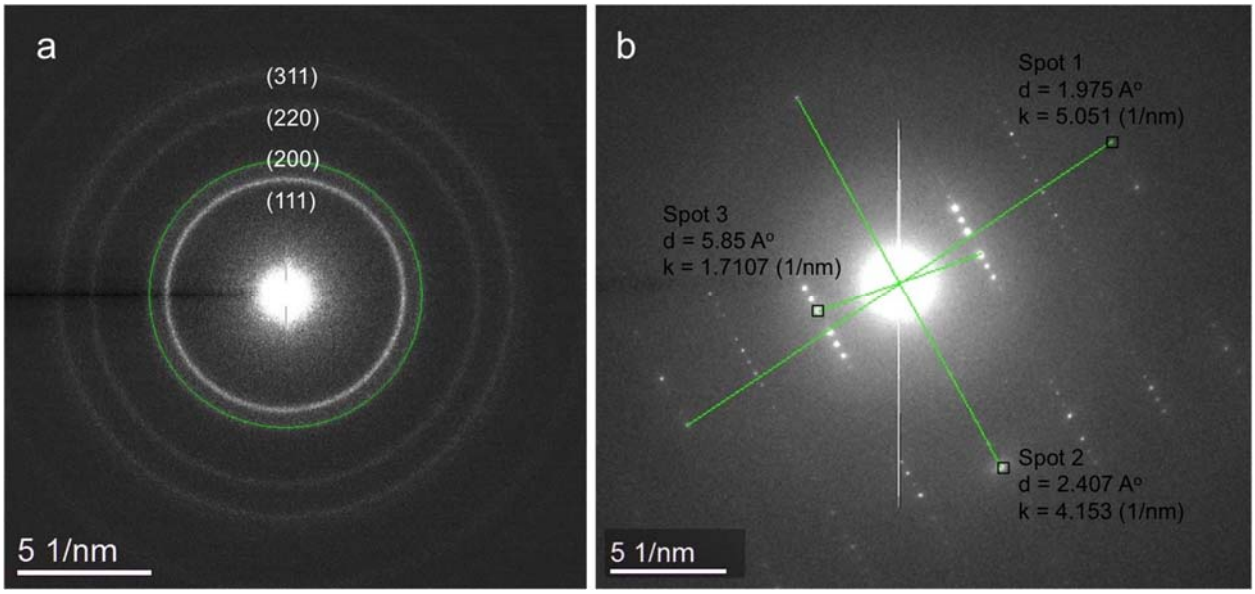

Table 17. Calculation of the calibration scale for the determination of the d and k values.

Miller Indices(hkl)	d-spacing (nm)	Calculated k (1/nm)	Determined k value from ring DP (1/nm)	Calibration scale (1/nm)
(111)	0.2359	4.239	4.351	0.01026868
(200)	0.2039	4.904	4.984	0.01039049
(220)	0.1442	6.934	7.0965	0.01031819
(311)	0.1229	8.136	8.2795	0.01037697

The measured d spacing and respective reciprocal distances k are tabulated in table 18.

Table 18. Measured k and d values of the three spots chosen for radiation damage study of a single crystal DPP polymer.

Spots	d spacing (A^o)	k (1/nm)
Spot 1	1.975	5.061
Spot 2	2.407	4.153
Spot 3	5.85	1.707

3.4 Radiation Damage Study of the DPP Polymer in JEOL 1400(120KeV) at -175℃.

Until now all the experiments are performed at room temperature. Reducing the temperature is one of the ways to reduce the damage in the beam sensitive specimens. Thus, we conducted an experiment at -175℃, which was achieved with the liquid nitrogen. For such experiments in the TEM, a special TEM cryogenic holder is utilized. After the setup, the rest of the imaging and analysis method remains the same as described earlier.

The figure 29 shows the area of imaging and diffraction pattern of the DPP polymer under the cryogenic conditions (-175℃). The complete experiment is performed at 120KV voltage and various dose rates.

Figure 29. a) Image area b) Diffraction pattern of DPP at 120KeV [-175℃].

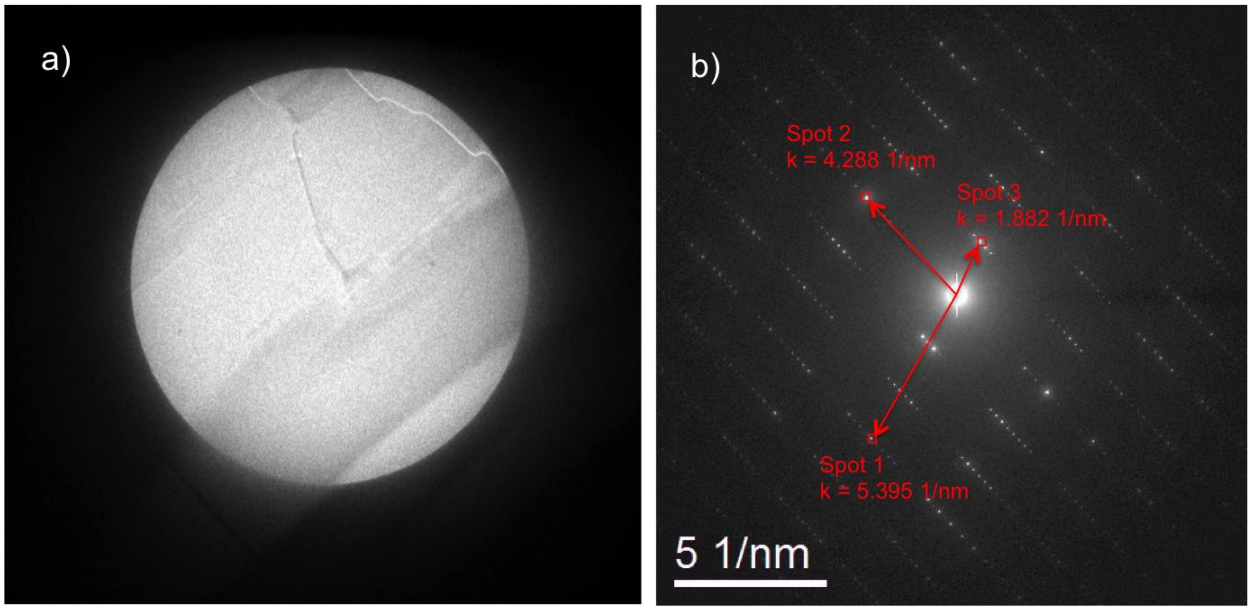

Results and Discussions

At first we conducted a study at a low dose rate of 0.0023785($\frac{e^-}{A^{o^2}.sec}$). Figure 30 show that it takes around 2 hours and 45 minutes for complete disappearance of the spots. The three spots chosen are very close to the earlier three spots chosen for the study at room temperature for 120KeV and 200KeV electron energies. This is to maintain consistency over the sets taken for the experiment. In figure 31, we can see how the mean intensity of the selected spots decreases exponentially at various electron doses. The critical dose values are calculated using Matlab exponential fit curves for the three spots.

The experiment is repeated for various dose rates increasing from the lowest. The mean critical dose values for the spot 1, spot 2 and spot 3 are 3.59, 5.17 and 7.29 respectively. The mean critical dose value for the spot 3 has increased almost three times at -175℃, than the value, which we got at the same electron energy of 120KeV and at room temperature.

Thus, here we conclude that for the DPP polymer lowering of temperature increases its resistance towards radiation damage.

Figure 30. Disappearance of the spots in the DPs for the a low dose study at 120 KeV and -175℃

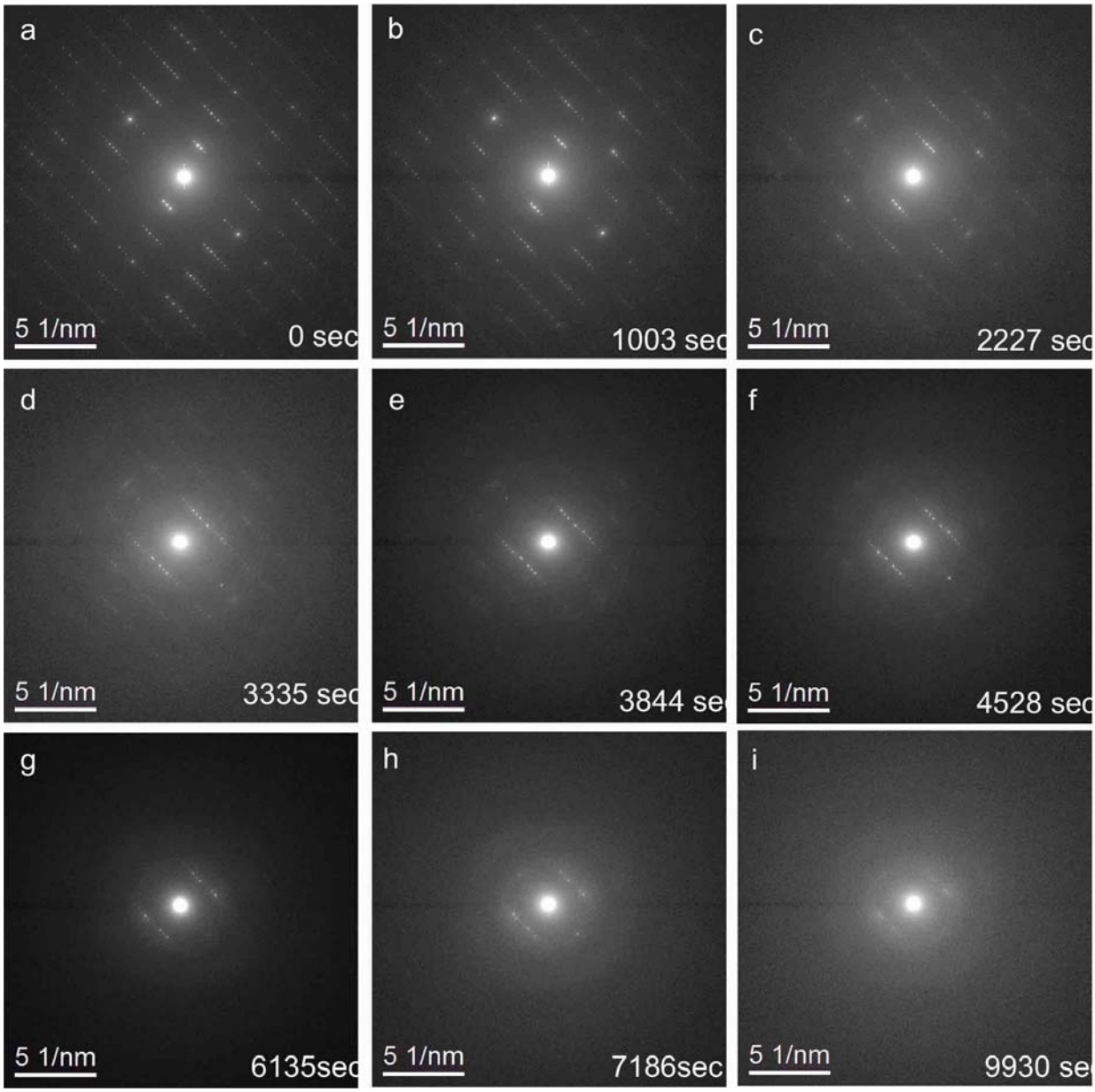

Figure 31. Mean Intensity vs. Electron Dose for the low dose rate study at 120KeV and -175℃

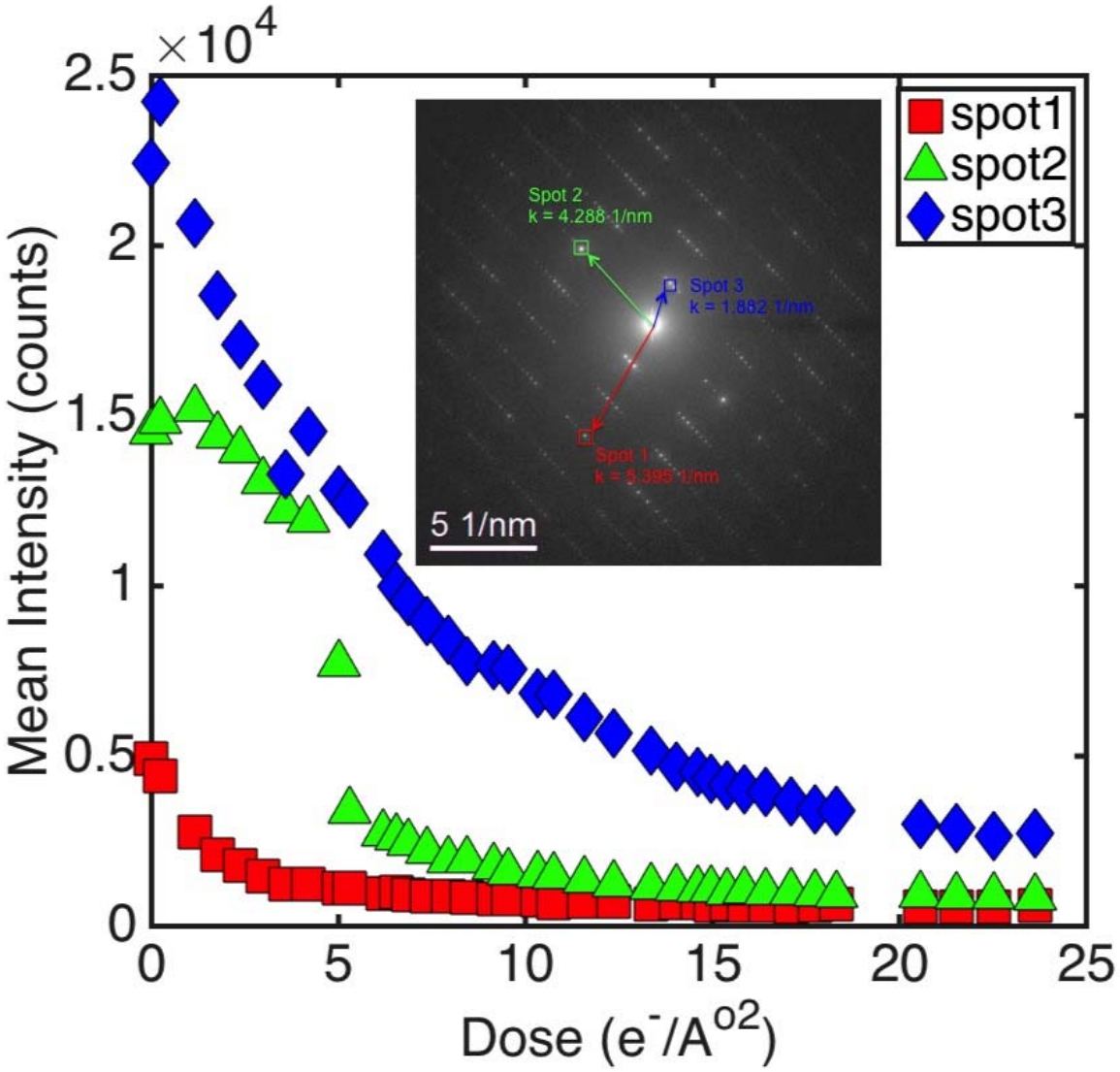

Table 19. Critical Dose values ($\boldsymbol{D_e}$) for various dose rates at 120KeV and -175℃

Dose Rate $(\frac{e^-}{A^{o2}.sec})$	$D_e\left(\frac{e^-}{A^{o2}}\right)$ (Spot 1)	$D_e(\frac{e^-}{A^{o2}})$ (Spot 2)	$D_e(\frac{e^-}{A^{o2}})$ (Spot 3)
0.0023785	2.11	4.41	6.21
0.0271	5.43	5.27	3.43
0.0273	4.16	----	7.45
0.0327	4.76	7.42	13.55
0.0345	1.22	6.6	10.6
0.0393	5.44	----	5.81
0.0724	2.06	2.17	8.25

Chapter 4

Conclusions

4.1 Critical Dose versus k (reciprocal space)

From the Table 9, Table 16, and Table 19 we can generate a graph of critical dose vs. the distance of the spots in k (reciprocal) space.

Figure 32. Critical Dose ($\boldsymbol{D_e}$) $\boldsymbol{vs.k}$ ($\frac{\mathbf{1}}{\boldsymbol{nm}}$) at 120KeV and 200KeV.

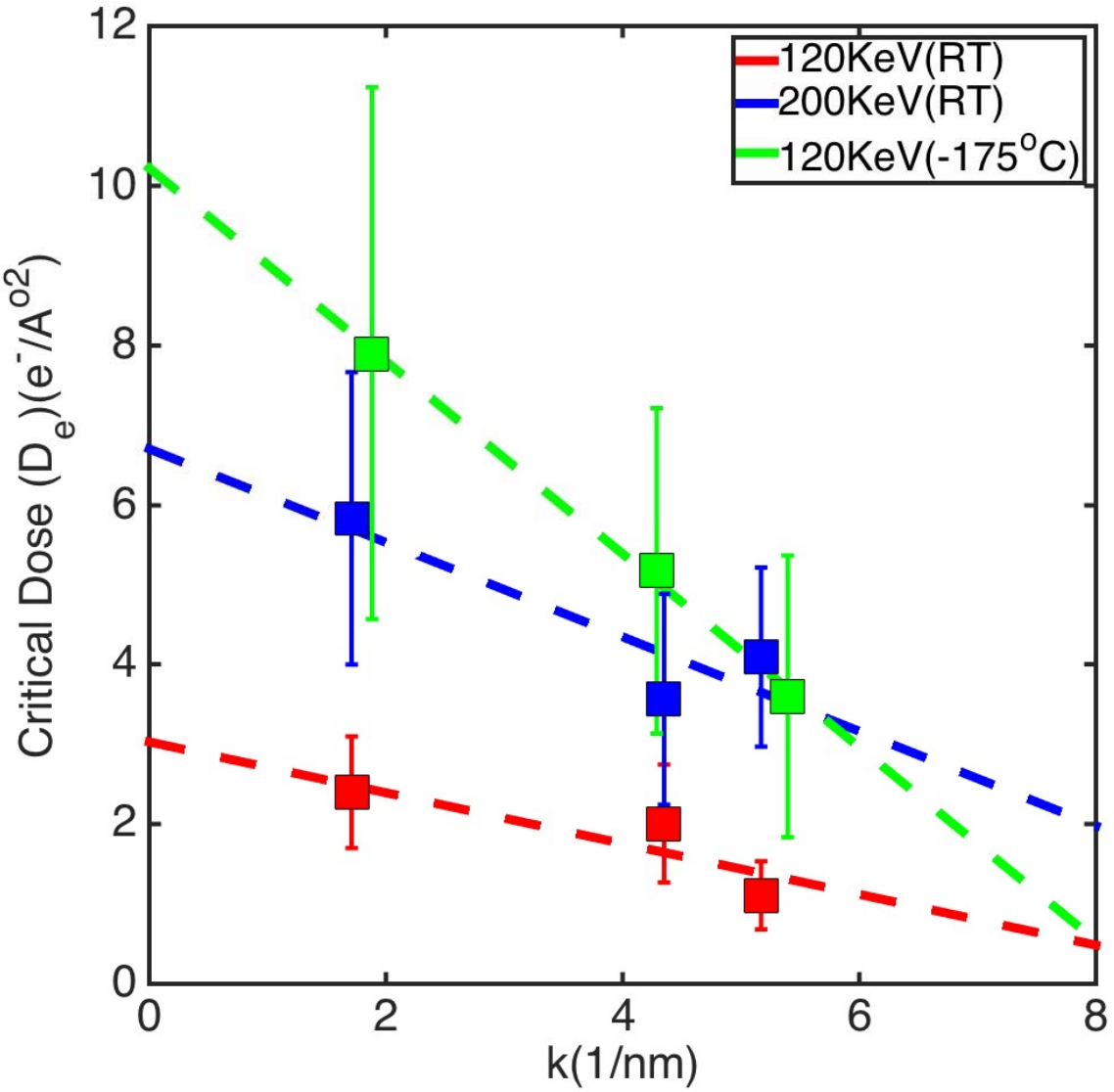

Earlier we concluded that the critical dose doesn't depend upon the dose rate value. Now from the above graph it is clear that the critical dose value increases for the selected three spots at higher electron energy. Also, we find that the critical dose value decrease almost linearly with the reciprocal space k. The approximated critical dose value is 6 ($\frac{e^-}{A^{o2}}$) at 200KeV and 3($\frac{e^-}{A^{o2}}$) at 120KeV. As the overall scattering decreases with increase in the electron energy, we find that the damage caused by the inelastic scattering is less at 200KeV than at 120KeV. The damage mechanism of the DPP polymer can be attributed to radiolysis or ionization, which causes the breakage of bonds leading to loss of the crystalline structure, which we have observed through the electron diffraction patterns.

We also performed an experiment to determine the critical dose value at a lower temperature of -175℃ by utilizing liquid nitrogen. The critical dose value at 120KeV and -175℃ is 8($\frac{e^-}{A^{o2}}$). Though reducing the temperature may not cause any effect to the inelastic scattering, but we do find the critical dose to increase. Therefore, we confirm that reducing the temperature is one of the ways to protect the polymers; in particular, the DPP based core polymers from the radiolysis damage.

Future work can be finding out the critical dose value at higher energy 300KeV.It will be interesting to find the magnitude by which the critical dose will increase.

References

1. Williams, D. and C.B. Carter, Inelastic Scattering and Beam Damage, in Transmission Electron Microscopy. 2009, Springer US. p. 53-71.
2. Williams, D. and C.B. Carter, Scattering and Diffraction, in Transmission Electron Microscopy. 2009, Springer US. p. 23-38.
3. Egerton, R., P. Li, and M. Malac, Radiation damage in the TEM and SEM. Micron, 2004. 35(6): p. 399-409.
4. Egerton, R., A Modest Proposal for the Propagation of Information Concerning Radiation Damage in the TEM, and as Fodder for Pasturized Professors. Microscopy Today, 2013. 21(06): p. 70-72.
5. Henderson, R. and R.M. Glaeser, Quantitative analysis of image contrast in electron micrographs of beam-sensitive crystals. Ultramicroscopy, 1985. 16(2): p. 139-150.
6. Egerton, R.F., S. Lazar, and M. Libera, Delocalized radiation damage in polymers. Micron, 2012. 43(1): p. 2-7.
7. Egerton, R. and I. Rauf, Dose-rate dependence of electron-induced mass loss from organic specimens. Ultramicroscopy, 1999. 80(4): p. 247-254.
8. Malis, T., S. Cheng, and R. Egerton, EELS log-ratio technique for specimen-thickness measurement in the TEM. Journal of electron microscopy technique, 1988. 8(2): p. 193-200.
9. Li, P. and R.F. Egerton, Radiation damage in coronene, rubrene and p-terphenyl, measured for incident electrons of kinetic energy between 100 and 200 kev. Ultramicroscopy, 2004. 101(2–4): p. 161-172.
10. Misra, M. and R.F. Egerton, Assessment of electron irradiation damage to biomolecules by electron diffraction and electron energy-loss spectroscopy. Ultramicroscopy, 1984. 15(4): p. 337-344.
11. Cazaux, J., Correlations between ionization radiation damage and charging effects in transmission electron microscopy. Ultramicroscopy, 1995. 60(3): p. 411-425.
12. Egerton, R.F., Choice of operating voltage for a transmission electron microscope. Ultramicroscopy, (0).
13. Howells, M.R., et al., An assessment of the resolution limitation due to radiation-damage in X-ray diffraction microscopy. Journal of Electron Spectroscopy and Related Phenomena, 2009. 170(1–3): p. 4-12.
14. Xue, G., et al., Ambipolar charge transport of TIPS-pentacene single-crystals grown from non-polar solvents. Materials Horizons, 2015.
15. Stolle, C.J., T.B. Harvey, and B.A. Korgel, Nanocrystal photovoltaics: a review of recent progress. Current Opinion in Chemical Engineering, 2013. 2(2): p. 160-167.
16. Li, H., et al., Solution-Grown Organic Single-Crystalline Donor–Acceptor Heterojunctions for Photovoltaics. Angewandte Chemie, 2015. 127(3): p. 970-974.
17. Zhang, Y., et al., Organic Single-Crystalline p−n Junction Nanoribbons. Journal of the American Chemical Society, 2010. 132(33): p. 11580-11584.
18. Li, H., et al., Solution-grown aligned C60 single-crystals for field-effect transistors. Journal of Materials Chemistry C, 2014. 2(18): p. 3617-3624.
19. Fan, C., et al., Solution-Grown Organic Single-Crystalline p-n Junctions with Ambipolar Charge Transport. Advanced Materials, 2013. 25(40): p. 5762-5766.

20. Li, H., et al., High-Mobility Field-Effect Transistors from Large-Area Solution-Grown Aligned C60 Single Crystals. Journal of the American Chemical Society, 2012. 134(5): p. 2760-2765.
21. Shi, H., et al., Effect of end-groups on the photovoltaic property of diphenyl substituted diketopyrrolopyrrole derivatives. Synthetic Metals, 2014. 188(0): p. 66-71.